NPL REPORT CMAM 034

REPORT

Review of methods for low frequency transducer calibration in reverberant tanks

S P Robinson

June 1999

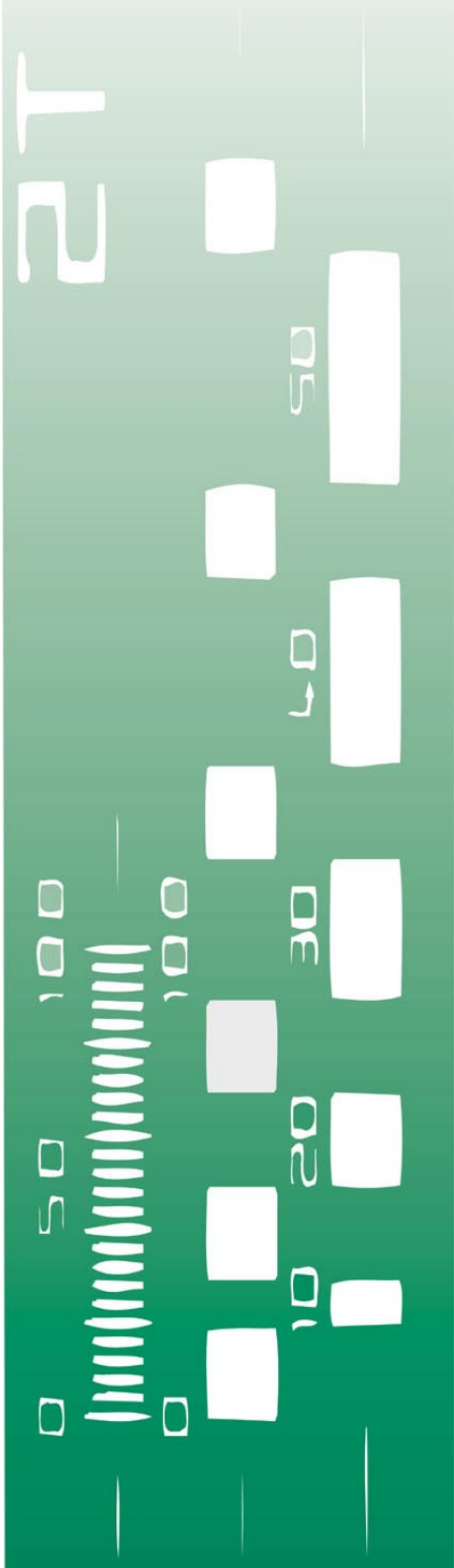

NPL
National Physical Laboratory

REVIEW OF METHODS FOR LOW FREQUENCY TRANSDUCER CALIBRATION IN REVERBERANT TANKS

Stephen Robinson

ABSTRACT

This report forms a deliverable of Project 2.1d(ii)(b) of the 1995-8 NMS Acoustics Programme.

A review is presented of different methods for calibrating underwater electroacoustic transducers in reverberant test tanks. Emphasis is placed on the use of novel techniques in situations where conventional methods breakdown, in particular for the calibration of acoustic projectors.

Techniques covered include the use of spatial and temporal averaging, using various types of noise as a source, modelling and extrapolating from the free-time signal, suppression of the transducer transient behaviour, the use of directional receivers and arrays, using various methods of echo elimination using signal processing, and attempts to model the reverberant acoustic field inside the test tank. For each method, full reference is made to the relevant literature on the subject. Although a full assessment of accuracy has yet to be undertaken on many of the methods, where possible an indication has been given as to the likely sources of error.

ISSN 1369-6785

National Physical Laboratory
Queens Road, Teddington, Middlesex, TW11 0LW

Approved on behalf of the Managing Director, NPL
by Dr G.R.Torr, Head, Centre for Mechanical and Acoustical Metrology.

CONTENTS

1. INTRODUCTION

1.1 BACKGROUND

In underwater acoustics, electroacoustic transducers are commonly used to generate and/or detect acoustic fields. If meaningful and quantitative underwater acoustic measurements are to be made, the transducers must be calibrated in a manner traceable to national standards. The free-field calibration of a hydrophone requires the determination of its electrical response to an incident acoustic plane-wave from a given direction. For a projector, a measurement is required of the acoustic pressure produced in a given direction and at a specified separation distance for a known electrical stimulus. For free-field calibrations, measurements must be made in a free-field environment which means there can be no interference from boundary reflections [1, 2].

For continuous wave fields, this requires the use of a large volume of water such as a lake, reservoir or ocean in order that reflections from the medium boundaries are sufficiently attenuated by propagation losses. Such facilities are not readily available, and their impracticality and expense has led to the use of laboratory tanks for measurements, with gated signals and time-windowing used to isolate reflections. Laboratory tanks have the advantage of more controlled experimental conditions, but their use introduces further measurement problems, especially at frequencies where the tank dimensions are small when measured in acoustic wavelengths.

The ability to perform calibrations and measurements in laboratory tanks is of particular interest to researchers in the marine acoustics industry since it enables testing to be done in-house without the need for measurements on open-water facilities or by use of very expensive sea-trials.

For a calibration method to be useful, it must be capable of being used to determine the parameters that describe the operation of electroacoustic transducers. Of particular interest are:

(i) transmitting response;
(ii) receiving response;
(iii) directional response pattern;
(iv) electrical impedance.

The receiving response tends to be more straightforward to measure since standard receivers (hydrophones) tend to be very low-Q devices. At audio frequencies, small hydrophones can be calibrated using pressure calibration methods which are equivalent to free-field methods for acoustically hard devices small compared to the acoustic wavelength [3]. More difficult is a measurement of the transmitting response of projectors since this is often required for quite large, high power projectors, which by their nature are high-Q devices and take a long time to reach steady-state.

1.2 ORGANISATION OF REPORT

In this report, a review is presented of different methods for calibrating underwater electroacoustic transducers in reverberant test tanks. Emphasis is placed on the use of novel techniques for overcoming the limitations imposed by finite-sized tanks in situations where conventional calibration methods breakdown, in particular at frequencies close to the lower limiting frequency of the tank.

Not all the techniques described have been implemented at NPL, but for each method a full reference is made to the relevant literature on the subject. Where results are available from work at NPL, typical examples are given. In such a review, inevitably only a relatively brief description of each method can be given. The reader is referred to the appropriate references for more detailed information. Although a full assessment of accuracy has yet to be undertaken on many of the methods, where possible an indication has been given as to the likely sources of error.

A description is first given of the limitations in the use of conventional techniques in reverberant tanks (Section 2). A description is then given of some of the methods used to overcome the low frequency limitations, such as broadband reverberant techniques (Section 3), methods utilising (or attempting to eliminate) the initial transient part of the acoustic waveform (Section 4), and methods using arrays of transducers (Section 5). Where appropriate, an indication has been given in the text of which of the parameters listed in Section 1.1 the method might be used to measure.

For a more detailed description of the general methods used in the calibration and testing of underwater acoustic transducers, the reader is referred to the excellent texts by Bobber [3] and Giangreco [4].

2. CONVENTIONAL CALIBRATION METHODS

2.1 BACKGROUND

To use finite-sized tanks in the free-field calibration of underwater acoustic transducers, a way must be found to eliminate the effect of boundary echoes (or at least to control or limit their influence). One method is to coat the boundaries with perfect absorbers, a method often attempted in airborne acoustics. However, efficient absorbers for underwater sound are expensive and rarely provide sufficient absorption over a wide frequency range. Consequently, the most common method adopted is to use electronic gating techniques to gate the transmit and receive signals, isolating the direct signal in the time-domain before the arrival of reflections. Absorbers are then sometimes used to reduce the overall reverberation time of the tank, allowing faster signal repetition rates.

During the calibration of transducers using this method, two transducers, one acting as a transmitter and the other as a receiver, are suspended in a tank of finite size filled with water. The transmitter sends an acoustic signal consisting of a tone-burst of finite duration. The signal received by the receiving hydrophone is contaminated by transients due to the resonance of the devices, and reflections of the transmitted signal from the tank walls and floor, and the water-air boundary. The received signal is sampled (in time), and it is required to estimate from these measurements the *steady-state* behaviour of the receiving and transmitting devices. Figure 2.1 shows typical examples of hydrophone signals measured during a calibration showing the transient signal, steady-state and reflections.

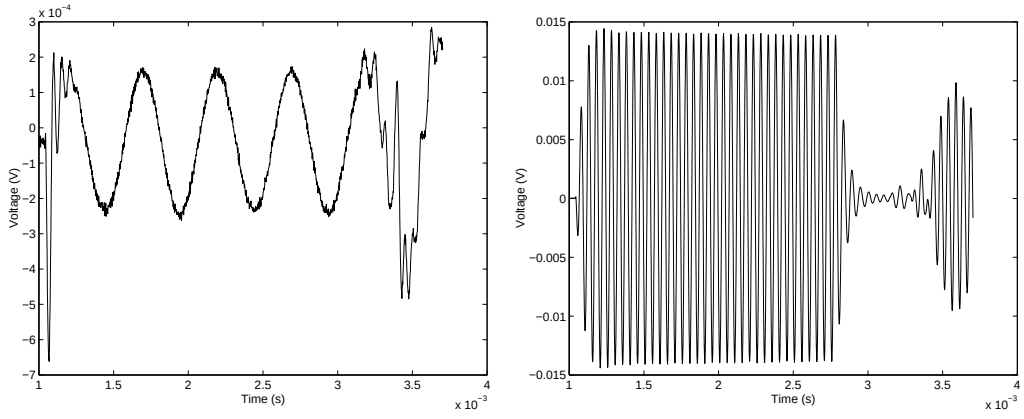

Figure 2.1 Measured data for the ITC1001 transducer corresponding to a 2 kHz drive voltage (left), and a 20 kHz drive voltage (right) with no electronic filtering applied.

The effects of transients and reflections are made worse at low frequencies because there are fewer complete cycles in the transmitted signal. Consequently, direct measurement of the steady state portion of the received signal is less reliable, and this imposes a lower bound (dependent on the tank size) on the range of frequencies over which hydrophones may be calibrated. A number of methods for reducing this bound, without the need for a larger tank, have been proposed and are sometimes referred to as "reverberation-limited" calibration

methods. This report consists of an appraisal of a number of these calibration methods, some of which require measurements to be made in the echo-free time available before reflections arrive at the receiver, and some which require measurements to be made in a reverberant field.

2.2 ECHO-FREE TIME

In Figure 2.2, a schematic is shown of two transducers in a reverberant tank illustrating the sources of echoes from the boundaries.

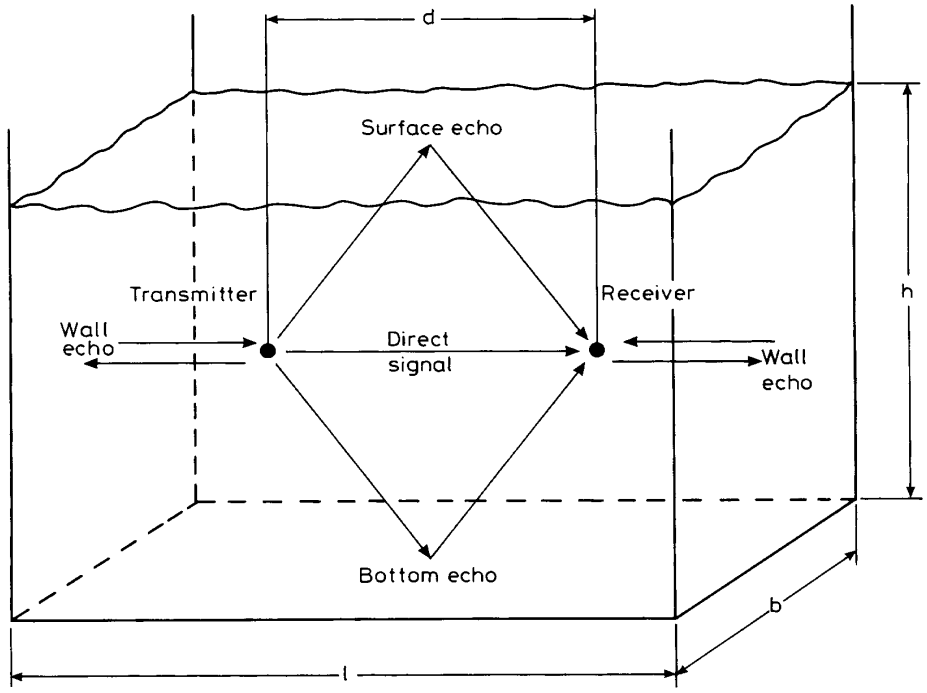

Figure 2.2 Schematic diagram of a projector and receiver in a water tank showing the main sources of reflections (ignoring multiple reflections).

By simple geometrical considerations (and knowing the speed of sound in water), it is possible to calculate the arrival time of the echoes and therefore the amount of time-domain signal available for analysis before the arrival of echoes [5]. This has been done for the NPL wooden tank and the results are shown in Figure 2.3. This tank is in fact a circular tank 5.5 m diameter and 5 m deep but the analysis is essentially similar to that for a rectangular tank. In addition to the boundary reflections, also shown are the reflections between transducers (standing waves) which are usually only significant for plane-faced transducers.

The analysis of Figure 2.3 is for two transducers positioned on a diameter of the tank, equi-spaced about the centre. As can be seen, an echo-free time of about 2.5 ms is available to observe the steady-state signal at separation distances of 1.8 to 2.0 m.

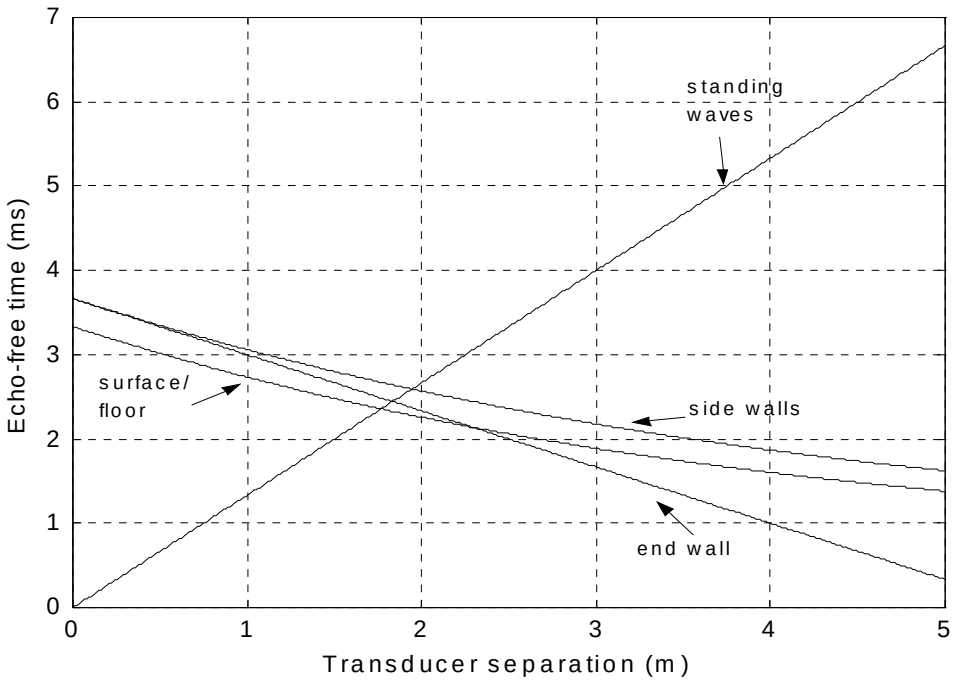

Figure 2.3 Echo-free time in the NPL wooden tank as a function of separation distance for two optimally placed transducers with sources of reflections marked. The echo-free time at any separation distance is given by the lowest valued line or curve.

2.3 CONVENTIONAL ANALYSIS METHODS FOR TONE-BURST SIGNALS

In the case of the signals shown in Figure 2.1, there is enough free-time before the arrival of the first echoes for the steady-state signal can be observed directly. Typically, a time-window or gate is applied so that only the portion of the steady-state signal within the window is made available for analysis. There are a number of ways of measuring the amplitude of the steady-state component that are in common usage. These include:

(i) Direct measurement of the peak voltage, either by a peak detector or by measuring the maximum and minimum of the digitised signal.

(ii) Calculating the RMS voltage (by squaring, averaging and square rooting the digitised signal). Ideally, this is done using an integer number of cycles of the sinusoidal signal.

(iii) Performing a fast Fourier transform (FFT) of the signal and taking the amplitude of the spectrum at the drive frequency, again using an integer number of cycles.

(iv) Performing a “narrow-band” discrete Fourier transform (DFT) of the signal, calculating only the amplitude of the component at the drive frequency, again using an integer number of cycles.

(v) Performing a least-squares fit of a sine-wave of the appropriate frequency and taking the amplitude of the fitted sine-curve.

All of the above methods have strengths and weaknesses. The peak measurement of (i) is simple to implement but inaccurate in the presence of any noise, distortion and residual amplitude fluctuations of the waveform envelope. The other methods all require a little more processing, perhaps with dedicated software algorithms. However, methods (ii) to (v) will provide some effective averaging of small amplitude variations if many cycles are contained within the time window. Methods (iii) to (v) will also provide some discrimination against noise and can also provide information on phase as well as amplitude. However, errors may occur with methods (ii) to (iv) if an integer number of cycles is not used for the analysis. Also, with the FFT of method (iii), an error may occur if the spectrum does not contain a point at the exact frequency of excitation. At NPL, methods (ii), (iv) and (v) are generally used depending on the number of cycles available for analysis. Both method (iv) and (v) can still be useful even when analysing only half a cycle of signal.

2.4 CONVENTIONAL FREE-FIELD CALIBRATION METHODS

The most common primary method of free-field calibration used in laboratory tanks is the method of three-transducer spherical-wave reciprocity [1-3]. This requires the use of three transducers, P, T and H, at least one of which must be a reciprocal transducer; that is, its transmitting and receiving sensitivities are related by a constant factor termed the reciprocity factor. The hydrophones are paired off in three measurement stages, at each of which one device is used as a transmitter and the other a receiver. For each pair of hydrophones, a measurement is made of the ratio of the voltage across the terminals of the receiving device to the current driving the transmitting device, this ratio being termed the transfer impedance, *Z*. By use of the reciprocity principle as applied to the reciprocal transducer, the sensitivity of any one of the three hydrophones can be determined from these purely electrical measurements as follows [1]:

$$M_H = \sqrt{J \frac{d_{PH}\, d_{TH}}{d_{PT}} \frac{Z_{PH}\, Z_{TH}}{Z_{PT}}} \qquad (2.1)$$

where M_H is the receive sensitivity of transducer H, d_{PH} is the separation distance between P and H, etc, and Z_{PH} is the transfer impedance when transmitting with P and receiving with H, etc. For a spherical-wave field, the reciprocity parameter, *J*, is given by $J = 2 / \rho f$, where ρ is the water density and *f* is the acoustic frequency. The transmitting response of any one of the devices may also be described with a similar equation. For each measurement of voltage and current, one of the methods described in Section 2.3 is used to measure the amplitude of the steady-state portion of the tone-burst signal. Since the transfer impedance is a ratio of electrical quantities, systematic errors in the measurements may be eliminated by using the same measurement channel (preamplifier, filter, digitiser) for each, and calibrated attenuators may be used to equalise the signals to minimise errors from nonlinearities in the measurement chain. At NPL, a current transformer is used to measure the drive current, and it is the traceable calibration of this item along with the electrical attenuators which provides the traceability back to national standards of electrical measurement (the amp and ohm) [5].

If a transducer is available which has previously been calibrated by an absolute method, this can be used to calibrate another transducer by a comparison or substitution method. For example, the response of a test hydrophone, T, may be compared to that of a reference hydrophone, H, by exposing both to the same acoustic field and using:

$$M_T = \frac{V_T}{V_H} M_H \qquad (2.2)$$

where M_H is the sensitivity of the calibrated reference hydrophone, and V_T and V_H are the measured voltages corresponding to the test and reference hydrophones respectively. It should be remembered that the quantities in the above equation are likely to vary with frequency.

If a calibrated reference hydrophone is used to calibrate a projector, P, which produces a spherically-divergent acoustic field, then the transmitting voltage response, S_P, can be written as:

$$S_P = \frac{V_H\, d_{PH}}{V_P\, M_H} = \frac{Z_{PH}\, d_{PH}}{Z_P\, M_H} \qquad (2.3)$$

where V_H is the voltage across the hydrophone, V_P is the drive voltage of the projector, and Z_P is the electrical impedance of the projector, the right hand side of the equation being derived by the use of Ohm's law with respect to the projector and remembering that Z_{PH} is defined as V_H/I_P. Of course, by rearranging the above equation, one can express the hydrophone receive sensitivity in terms of the transmitting response of the projector, allowing a calibrated projector to be used to calibrate a hydrophone of unknown response.

At frequencies less than a few kilohertz, a pressure calibration may be performed on a small hydrophone by a number of methods which involve generating acoustic pressures in small couplers. For example, the method of coupler reciprocity or the use of pistonphones. Such methods provide sensitivities which are equivalent to free-field sensitivities for hydrophones which are small compared to the acoustic wavelength (and therefore omnidirectional). Other calibration methods applicable to low frequencies are those that use of some kind of travelling-wave tube. In general, all these audio-frequency methods are difficult to apply to projectors, which must be calibrated in a laboratory tank.

A description of such calibration methods is beyond the scope of this report since they do not generally involve measurements in water tanks. For an excellent description of such methods, the reader is referred to the text of Bobber [3].

2.5 BREAKDOWN OF CONVENTIONAL TECHNIQUES

In the examples from Figure 2.1, the steady-state signal can be observed directly. As might be expected, fewer cycles of the steady-state signal are available for analysis at lower frequencies since the period increases with decreasing frequency. If the echo-free time for a particular tank with transducers optimally positioned is denoted by T, then the number of cycles available for analysis before the arrival of reflections is equal to the product fT, where f is the frequency of excitation.

If these cycles are to be used for analysis, steady-state conditions must be reached if one of the

methods of section 2.3 is to be employed. Since the electroacoustic transducers used in underwater acoustics are resonant devices behaving as damped harmonic oscillators of quality-factor Q, it will take approximately Q cycles of the resonance frequency before the initial turn-on transients have died away. For situations where $Q > f\,T$, so that steady-state is not reached within the free-time available, *all* of the methods described in section 2.3 will lead to inaccurate values for the steady-state amplitude.

As an example, in the 5.5 m diameter by 5 m deep measurement tank at NPL, the echo-free time of about 2.5 ms allows 5 cycles of 2 kHz signal. For a resonant transducer of $Q = 10$ and resonant frequency of 2 kHz, the steady-state can never be observed directly and classic tone-burst and time windowing methods cannot be used successfully. Of course, for any given size of tank there will be a frequency (depending on the transducer Q-factor) where the accurate use of classical techniques becomes impossible. In such cases, other methods must be employed to achieve a successful calibration.

2.6 LOW FREQUENCY CALIBRATION METHODS FOR REVERBERANT TANKS

The remaining sections of this report describe *some* of the methods which have been reported in the literature for calibrating transducers in reverberant test tanks at low frequencies. What is regarded as low frequency depends on the size of tank but for typical tank sizes is in the range 500 Hz to 20 kHz.

Techniques covered include the use of spatial and temporal averaging, using various types of broadband signals as a source, using various methods of echo elimination using signal processing, modelling and extrapolating from the free-time signal, suppression of the transducer transient behaviour, and attempts to model the reverberant acoustic field inside the test tank. For each method, reference is made to the relevant literature on the subject. Although a full assessment of accuracy has yet to be undertaken on many of the methods, where possible an indication has been given as to the likely sources of error. One omission from the report is the use of near-field arrays for the calibration of transducers - this is beyond the scope of this report.

For those methods implemented at NPL, some typical results are presented. Examples of calibration results are given where measurements were made in a small test tank and then a comparison is made with measurements made in a larger tank where conventional tone-burst methods may be used. Clearly, the larger tank could simply be used for all the measurements, but the small-tank results are presented to illustrate the methods concerned. It should be noted that the methods presented in the following sections should *not* be regarded as replacements for conventional methods. Indeed, the accuracy of the techniques shown is likely to be much degraded compared to conventional free-field techniques. However, these techniques are useful to provide in-house calibrations of transducers, perhaps during prototype development, where testing at sea or in open-water facilities is not practicable or too expensive.

3. CALIBRATIONS IN CONTINUOUS WAVE ACOUSTIC FIELDS

The techniques summarised in this section involve the use of continuous signals for the calibration of acoustic transducers in reverberant tanks. Such calibrations are not true free-field calibrations since the measurements are undertaken in the presence of reflections from the boundaries of the medium. The analysis of the measured data is typically performed in the frequency domain, with signal processing ranging from simple averaging or smoothing to attempts at echo removal by various forms of deconvolution, windowing or filtering.

In the case of a source in a reverberant enclosure, at any point in the field we are interested not just in the reflection of one specified sound wave but the simultaneous reflection of many waves impinging from very different directions with very different amplitudes and phases. Instead of investigating each individual wave, we can assume that amplitudes of the incident waves to be distributed uniformly over all possible angles of incidence in such a way that each element of solid angle carries the same intensity. Furthermore, we can assume that the phases of the waves are distributed at random so that interference effects can be neglected and we can simply add their energies. The energies are proportional to the square of the pressure amplitudes of the elementary waves. This type of sound field is often referred to as *diffuse* (eg in the literature of room acoustics) [6, 7].

The acoustic field in a reverberant enclosure which has a canonical geometry (eg rectangular tank, cylindrical tank with flat ends) may be treated as the superposition of modes within the tank. If a broad-band signal is used to excite the tank, at sufficiently high frequencies (see Appendix A) the modal density is such that many modes will overlap in frequency and give rise to a relatively smooth spectrum which is much less dependent on position in the tank than would be the case for a narrow band excitation signal, reducing the error due to positioning inaccuracies. This is one reason why broadband signals (such as Gaussian noise) are commonly used in reverberant calibrations. They also have the added advantage of enabling a calibration to be made at a range of frequencies simultaneously.

It should be noted that the sensitivity in a perfectly diffuse field, M_D, may be related to that in a free-field, M_F, as follows [3]:

$$M_D = D_\theta \, M_F \tag{3. 1}$$

where D_θ is the directivity factor, the average of the directional response of the transducer over all angles of orientation where the directional response has been normalised to unity for the free-field sensitivity at $\theta = 0°$.

However, it is difficult to achieve a truly diffuse field in underwater acoustic test tanks since large volumes and low absorption boundaries are required The reverberation time, T, for the signal to drop by 60 dB is given by

$$T = 55.2 \, \frac{V}{c\,A} \tag{3. 2}$$

where V is the volume, c is the sound speed and A is the overall absorption of the tank, the constant of 55.2 being derived from the -60 dB definition. Concrete or steel test tanks have typical reverberation times of less than 1 second. Scaling for the difference in sound speed with air still gives less than 5 seconds, which compares poorly with the 12-15 second

reverberation times for reverberation chambers in airborne acoustics. The greater coupling between the water medium and the walls (giving greater loss) and the higher sound speed mean that large volumes would be required to achieve similar reverberation times.

However, although the calibrations may be undertaken in the underwater equivalent of a cathedral rather than a true reverberation chamber, a calibration which is representative of the free-field calibration can still be performed at low kilohertz frequencies where the transducers are almost omnidirectional (directivity factor ≈ unity). If a simple comparison calibration is being undertaken, then greater accuracy may be obtained if the devices used are of the same type (thus having similar directional response). Indeed, if the hydrophone were ultimately to be used for measuring a diffuse sound field (eg that of ambient noise), it may be considered that the diffuse field sensitivity may be of more relevance to the user.

Another potential source of error when calibrating projectors in reverberant fields is that the measured response may be directly influenced by the reflected wave through the radiation impedance of the transducer. This is particularly important for high-Q projectors driven at resonance where the radiation impedance is a substantial portion of the overall impedance.

3.1 METHODS USING SMOOTHING OR AVERAGING TECHNIQUES

The results of transducer calibration in a reverberant field will show the influence of acoustic reflections which manifest themselves as perturbations on the true free-field frequency response of the transducer under test.

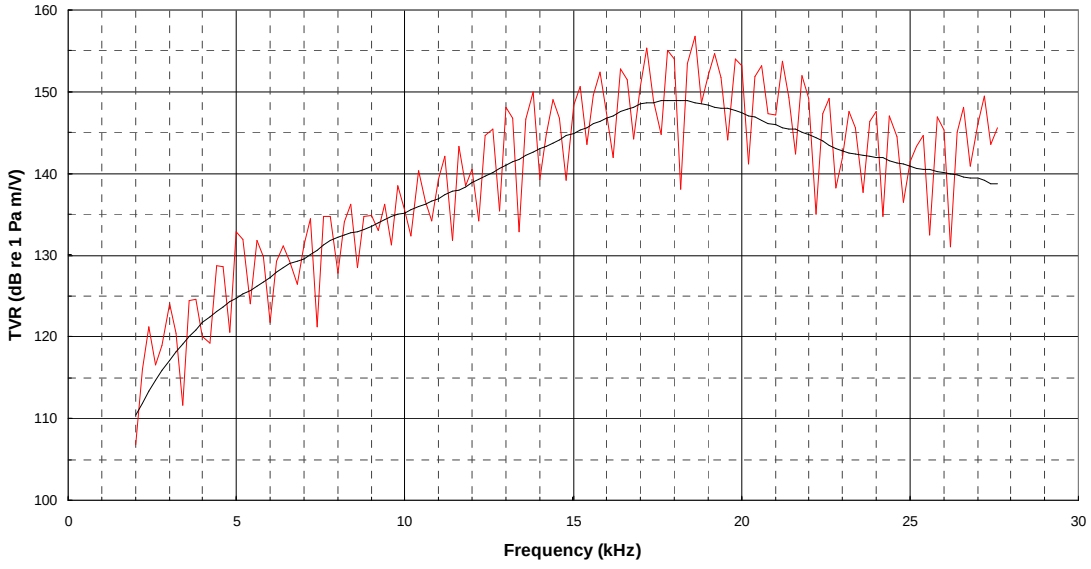

Figure 3.1 The transmitting voltage response of a transducer measured in a reverberant tank showing the influence of reflections. Also shown is the free-field response for comparison.

An example is given in Figure 3.1 of the transmitting voltage response of a transducer

measured in a small reverberant tank using a single frequency drive signal where the frequency has been varied in discrete intervals. Perturbations are clearly observed in the underlying smooth free-field response due to several boundary reflections.

3.1.1 Smoothing in the frequency domain

A number of methods have been reported which attempt to reduce or eliminate these perturbations. Perhaps the simplest is to attempt to smooth out the perturbations by fitting a smooth curve to the data to illustrate the underlying trend [3]. However, without knowledge of the true free-field response, it is difficult to apply this technique accurately, particularly in the presence of large perturbations from many reflections. Figure 3.2 shows the result of fitting a smooth curve to the data given in Figure 3.1. The curve fitting was done using NPL written software called NPLFIT, with the least-squares fit being achieved using cubic splines with three interior knots. The choice of fitting parameters (order of polynomial, number of knots, etc) was chosen to provide a smooth fit with one main resonance. The mean difference between the fitted curve and the free-field response is 1.6 dB. Also shown, but with poorer agreement with the free-field response, is a fitted curve where the data was first converted to linear units before performing the fit.

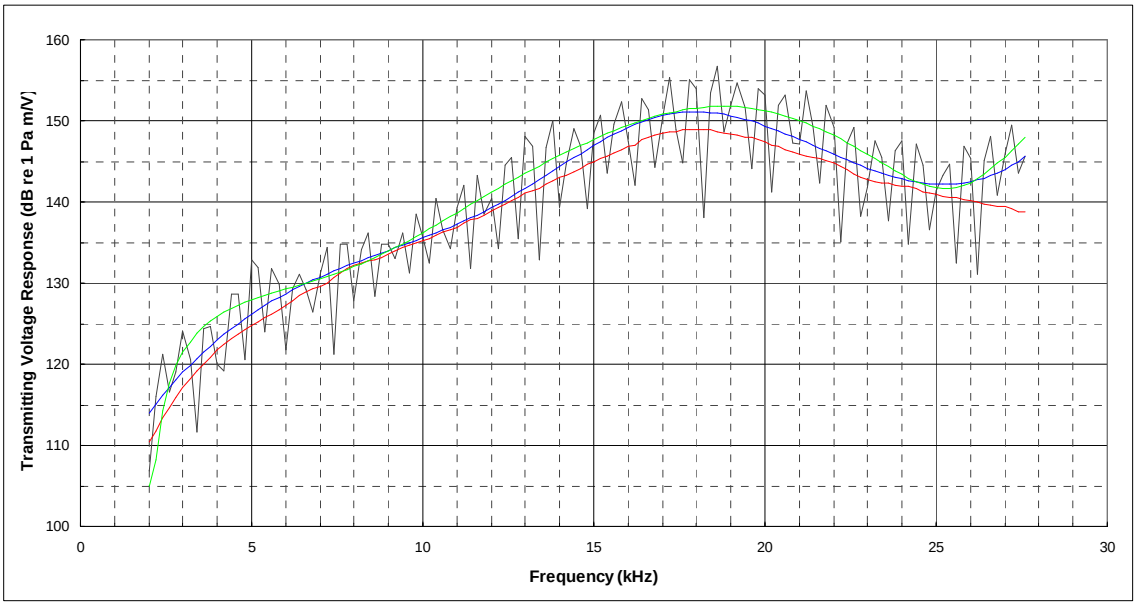

Figure 3.2 The results of fitting a curve using piece-wise cubic splines to the data already shown in Figure 3.1: (i) fit to the data in dB (blue); (ii) fit to the linearised data (green); (iii) for comparison, the true free-field response (red).

The accuracy of the results obtained using this smoothing method depend on the form of the data. In the example above, the calibration was performed in the presence of a maximum of two or three reflections. However, in the presence of many reflections, the data can exhibit even more fluctuations, some of which are much larger in amplitude and more difficult to smooth out since they will distort the fitted curve. Better results can be obtained if the fit is constrained by the use of *a priori* information about the transducer response. For example,

this might be done by specifying the number of turning points or positions of interior knots according to how many resonance peaks are known to exist in the free-field response. Additionally, the fit may be weighted to give less emphasis on data which are believed to deviate more strongly from the true response, or which show larger random uncertainty.

3.1.2 Spatially averaging the field to smooth the response

In general, an individual source of reflections at a distance Δd from the receiver will give rise to a periodic ripple on the frequency response, where the period in the frequency domain (spacing between adjacent peaks), Δf, is given by:

$$\Delta d = \frac{c}{\Delta f} \tag{3. 3}$$

where c is the sound speed. However, in the presence of many reflections, it difficult to use this relation directly to remove their influence. One method that may be adopted however is to make repeated measurements at different locations in the tank, since at each location the conditions for interference between the waves are different (this is equivalent to varying Δd in the above equation, thus altering the perturbations in the response). The mean of all the responses measured at many different locations should approach the free-field response.

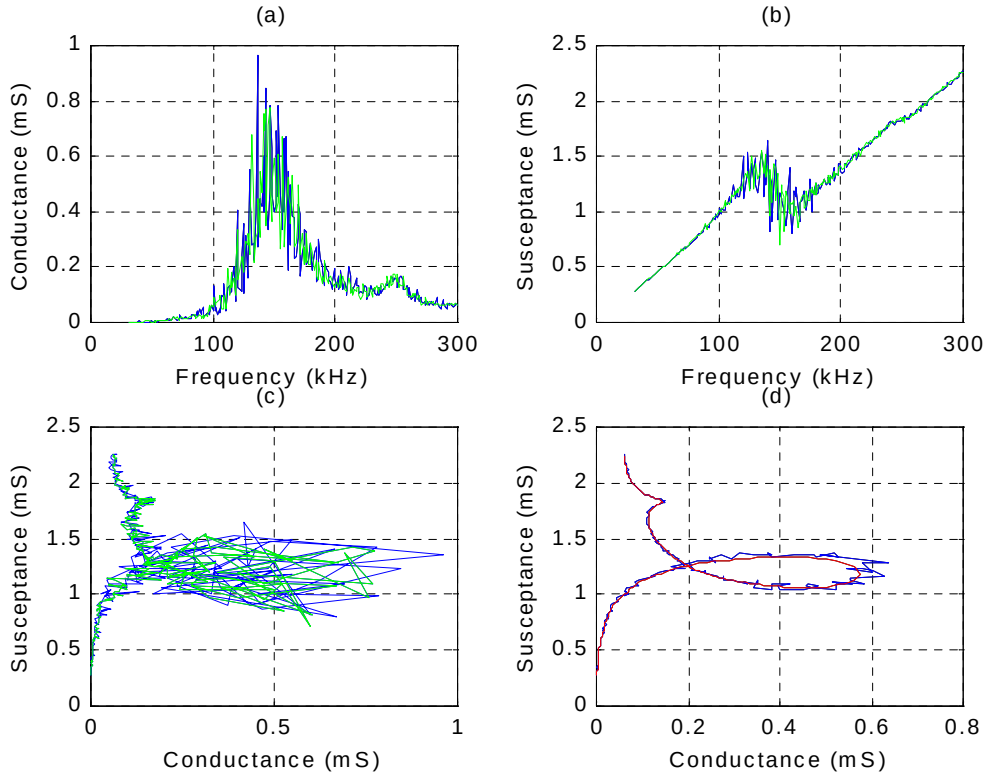

Figure 3.3 Results (a), (b) and (c) show admittance measurements of a transducer at two positions (green and blue curves) in a small measurement tank. Plot (d) shows the mean of data measured at 50 separate positions (blue) compared with the free-field response (in red).

This spatial-averaging technique has been used by Everitt [8] at the University of Bath, UK,

to eliminate the effect of echoes in the measurement of electrical impedance, some results of which are shown in Figure 3.3. To illustrate the technique, Everitt performed a frequency-scaled experiment using a small B&K8103 hydrophone measured in very small vessels where the hydrophone position could be easily controlled. An HP4192A impedance analyser was used to measure the admittance of the transducer using stepped continuous-wave sinusoidal excitation in the range 30-300 kHz. The results in Figure 3.3 were obtained from measurements in a pyrex beaker of only 12 cm diameter and 10 cm depth. Analogous results may be obtained by scaling the tank and transducer up in size and down in frequency.

To achieve acceptable results for the mean response, separate measurements were made at a total of 50 different positions in the tank. This requirement for a large number of measurements is a strong disadvantage of this method since it may not be practicable to make so many measurements, particularly when using large laboratory tanks and large transducers where altering the transducer position is not so easy without an automated positioning system.

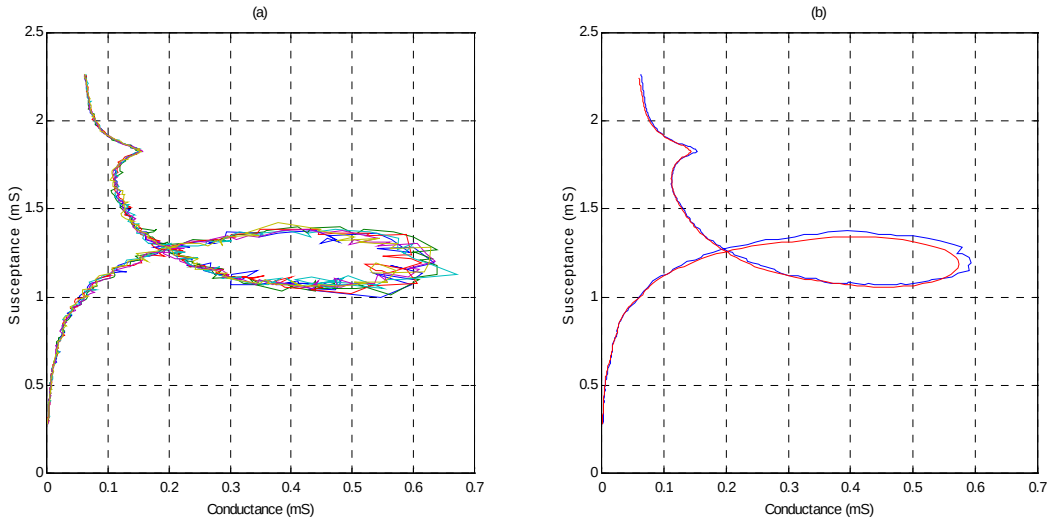

Figure 3.4 The plots in (a) show admittance measurements of a transducer at three positions (green, red and blue curves) in a small perspex measurement tank. Plot (b) shows the mean of data measured at 50 separate positions (blue) compared with the free-field response (in red).

Figure 3.4 shows some results for the same transducer made in a 10 x 18.5 x 6 cm rectangular perspex beaker. The individual show less perturbation since the perspex walls tend to absorb more of the sound leading to a less reverberant field. In such a case, fewer measurements are required to obtain an acceptable mean.

3.1.3 Smoothing/filtering in the time domain

Another method which has been used to eliminate the effects of the echoes, is to Fourier transform the frequency response data to calculate an “impulse” response of the transducer, and then window the data in the pseudo-time domain to eliminate the reflections which arrive at a later time than the direct path signal. After windowing, the data is transformed back to the frequency domain, whereupon a smoothed version of the initial response is obtained. This method has been successfully used by DCN, France, and is described as “temporal

smoothing" by Giangreco [4].

In summary, the technique involves applying the following transformations to the measured frequency response data, *y(f)*:

$$y(f) \xrightarrow{FT} y(t) \xrightarrow{Filter} y(t).W(t) \xrightarrow{FT^{-1}} y_S(f) \qquad (3.4)$$

where *W(t)* is a window function applied to the data in the time domain, $y_S(f)$ is the filtered or smoothed data, and *FT* and FT^{-1} represent taking a forward and inverse Fourier transform respectively. Figure 3.5 illustrates the use of this method at NPL for the data originally introduced in Figure 3.1. Plot (a) shows data after transforming to the time-domain with a strong reflection present after about 1.5 ms, and plot (b) shows the original data, the free-field response and the smoothed data which differs from the free-field response by between 1 and 3 dB in the frequency range 5 - 25 kHz.

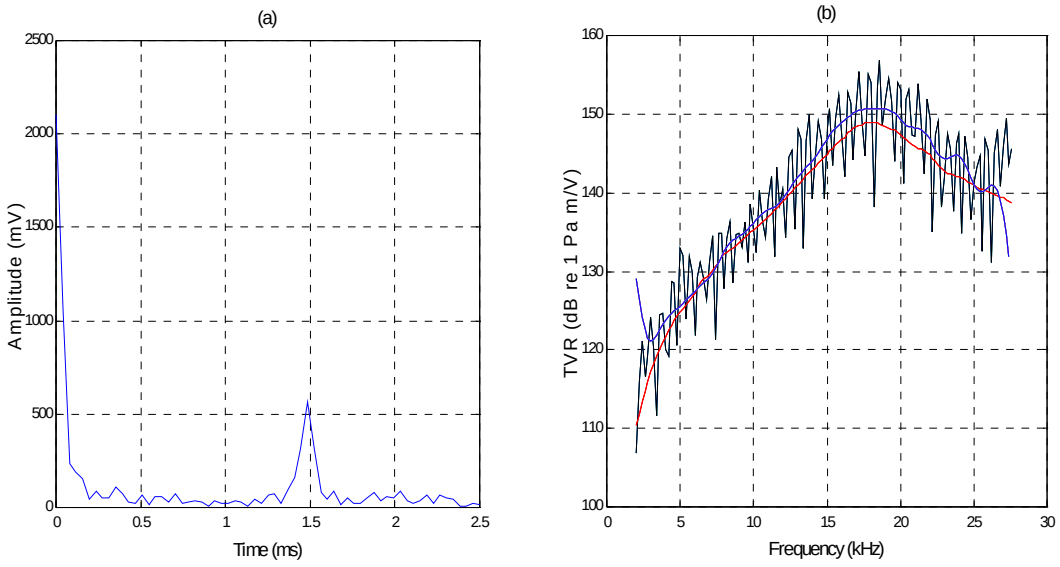

Figure 3.5 Results of smoothing in the time-domain: (a) the time-domain data before windowing; (b) comparison of the original data (black), free-field response (red), and smoothed response (blue).

Some of the perturbations in the smoothed response are caused by the fact that a rectangular time-domain window has been chosen in this case, leading to side-lobes in the frequency domain where the Fourier transforms of the window function and the data are convolved. This effect may be minimised by choice of another graduated window. Alternatively, the use of successive applications of windows of different duration, where the zeros in the spectrum of one window coincide with the peaks in the spectrum of another, can also help to eliminate these artefacts [4]. The method works best where there is only one or two strong reflections (eg from the water surface) and where the true response of the transducer under test is a smoothly varying function of frequency (any rapid fluctuations in the true response may be smoothed also). The method can be applied to the calibration of projectors or hydrophones.

3.2 CALIBRATION IN A RANDOM NOISE FIELD

A number of methods described here make use of broadband noise to generate an acoustic field for calibration. Perhaps the simplest such method is to perform a direct comparison or substitution calibration using such a field, and this method is discussed in some detail below. Many of the observations made about this method are common to the other methods described in later sections.

3.2.1 Method

The use of random noise as a signal in transducer calibration was reported as early as 1953 [9] but accuracy was limited by the processing technology available at the time. Since then, technological advances have enabled a variety of techniques utilising random signals to be employed. With the advancement in the performance of computers and signal analysers, the signal/data processing is not a serious limitation. In fact, modern signal analysers allow the automatic on-board calculation of fast Fourier transforms, cross and autocorrelation functions, coherence, etc, which greatly improves the speed of the calibration. Often, signal analysers also provide an output or signal source which can be used to provide the noise signal to drive the transmitting device.

The method consists of exposing the unknown hydrophone and a reference hydrophone to the same acoustic field, the reference hydrophone having been previously calibrated by an absolute calibration method [10]. The acoustic field is generated by a projector driven with a random noise signal and the analysis is performed in the frequency domain. The sensitivity as a function of frequency, $M_H(f)$, of the unknown hydrophone is calculated from:

$$M_H(f) = \frac{F_H(f)}{F_R(f)} M_R(f) \qquad (3.5)$$

where $M_R(f)$ is the sensitivity of the reference hydrophone as a function of frequency, and $F_H(f)$ and $F_R(f)$ are the spectra of the signals measured by the unknown and reference hydrophone respectively.

It is important to employ some signal averaging to smooth the spectra during the measurement process and of course, this must be undertaken in the frequency domain rather than the time domain. Up to 100 spectra may be averaged to obtain the data for use in calculations.

3.2.2 Coherence considerations

An important consideration with such a method is whether the pressure experienced by each hydrophone is the same. A good indicator of whether this is the case is to examine the coherence function, $\gamma_{xy}^2(f)$, which is defined as:

$$\gamma_{XY}^{\ 2} = \frac{|G_{XY}(f)|^2}{G_{XX}(f)\,G_{YY}(f)} \qquad (3.6)$$

where $G_{XY}(f)$ is the cross spectral density between the two signals, and G_{XX} and G_{YY} are the

power spectral densities of each signal respectively. For two coherent signals, the coherence will be unity and the degree to which the coherence is less than unity will provide an indication of the validity of the assumptions within the method. If an attempt is made to plot a smooth curve through the measurement results, the coherence may be used to provide a weight for each data point.

In Figure 3.6, a number of typical coherence functions are shown measured for an ITC1001 projector being driven with Gaussian random noise using two hydrophones positioned within a few cm of each other in the test tank. The coherence shown in plot (a) was measured in the NPL 5.5 m diameter wooden tank and shows good coherence down to about 500 Hz. The coherence plots shown in (b) were measured at two separate positions in NPL's smaller 2 x 1.5 x 1.5 m GRP tank and illustrate that the coherence can vary with position in the tank.

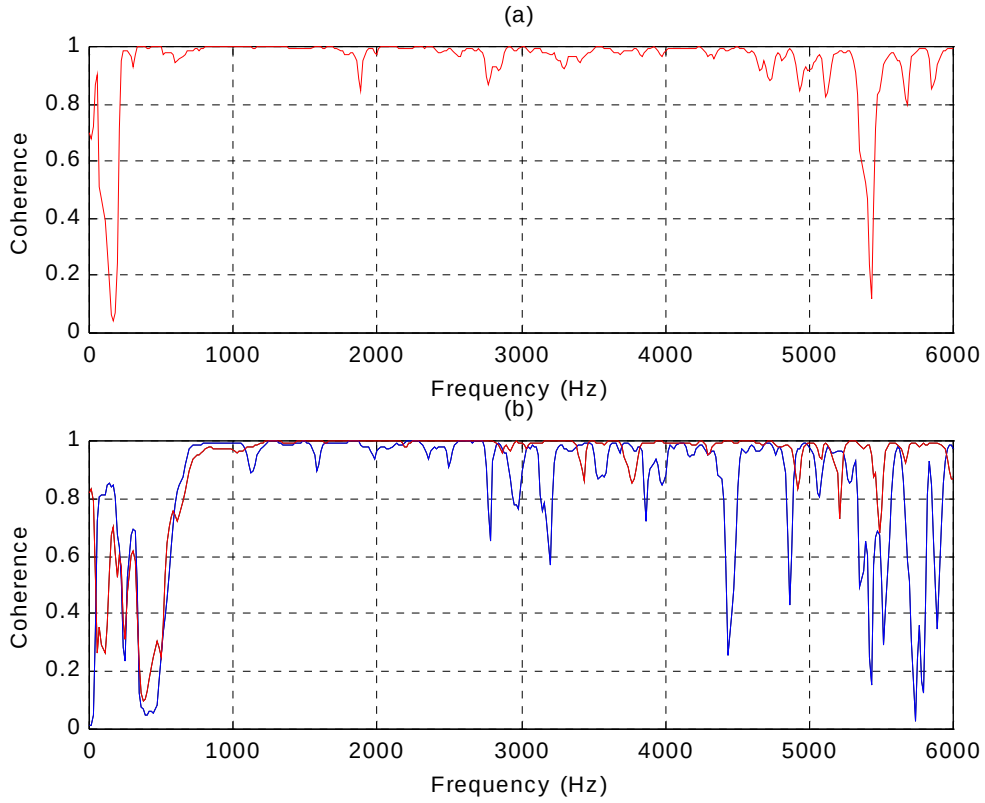

Figure 3.6 Coherence measurements in (a) the NPL 5.5 m diameter tank, and (b) at two positions in the 2 x 1.5 x 1.5 m tank measured using a TC4023 and B&K8104 hydrophone, with an ITC1001 projector driven by Gaussian random noise (100 kHz bandwidth).

3.2.3 Practical considerations

Signals such as Gaussian random noise may be generated using a specific noise generator (eg the B&K 1405 noise generator), an arbitrary waveform generator or even using the internal source of a signal analyser such as the HP89410A. If the source is digital, a pseudo-random noise signal may be generated digitally using a random number generator. This has an advantage in that, since it is actually deterministic rather than random, it can be replayed

repeatedly which can give benefits for signal averaging. Other signals that have been used include linear frequency-modulated sine wave signals.

In the procedure for measurements, in order to ensure that the two hydrophones experience the same acoustic pressure it is common for both of the hydrophones to be placed in the water tank simultaneously and positioned close together. This allows the signals from the two devices to be captured simultaneously, the coherence to be calculated as a check on the validity of the method, and the difference of the spectra to be calculated automatically on-board the signal analyser. The disadvantage of simultaneous measurement is that the two hydrophones cannot be positioned at exactly the same point in the tank/field and there is the potential for the presence of one device to influence the pressure sensed by the other.

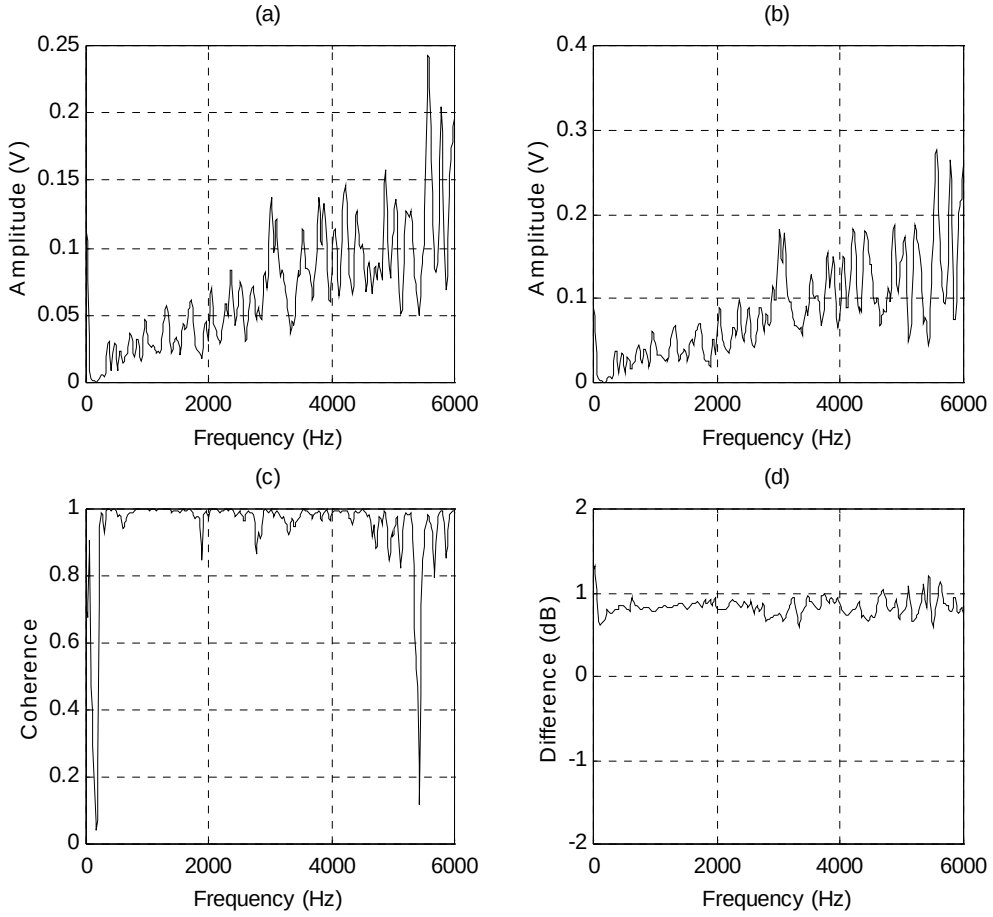

Figure 3.7 Measured spectra from TC4023 reference hydrophone (a) and a B&K8104 (b), along with the measured coherence (c), and the difference spectra (d). An ITC1001 was used as the projector driven with Gaussian random noise.

An alternative procedure is to undertake successive measurements on each of the hydrophones using a substitution or replacement technique. This procedure has the disadvantage that it takes longer, and does not expose both devices to the same field simultaneously (which is the ideal), and does not provide two simultaneous signals to be used

in the calculation of the coherence function. However with sufficient averaging in the frequency domain, acceptable results can be obtained - in the small 2.0 x 1.5 x1.5 m tank at NPL, reproducibility of 0.5-1.0 dB has been obtained in the frequency range 0.8 - 10 kHz. The substitution method is improved if a digitally generated pseudo-random signal is used since this may be stored and re-transmitted to both devices, ensuring the same field is experienced by each.

In practice, in tanks of symmetrical shape (eg rectangular sectioned or cylindrical with flat ends) it is better to position the transducers asymmetrically in the tank, thus keeping them away from any nodes due to major low frequency modal structure within the tank. A good practice is to repeat the calibration at a number of transducer positions in the tank since averaging the results will average the effects of any variation of results with transducer position. The method can be applied to the calibration of a projector also, but in this case the spectrum of the drive signal must be measured as well as that of the reference hydrophone and the separation distance between the transducers.

Figure 3.7 (a) and (b) shows examples of spectra of the signals from two hydrophones measured in the 5.5 metre tank at NPL. The projector used was an ITC1001 transducer driven with Gaussian random noise, the signals being captured on an HP89410A vector signal analyser. The reference hydrophone was a Reson TC4023, the unknown hydrophone under calibration being a Brüel & Kjær 8104. Figure 3.7 (c) shows the coherence signal and (d) shows the difference of the two spectra. At the low frequencies of 1-6 kHz used, the hydrophones are relatively omnidirectional. Note that smooth results are obtained down to frequencies of around 500 Hz.

3.2.4 Discussion

This method can be used to cover a broad frequency range from hundreds of hertz to several kilohertz, is quick to implement and can provide magnitude and phase information. The method can be used for determining the sensitivity of a transmitter or receiver, and may even be applied to an absolute reciprocity calibration. With care, agreement with free-field calibrations of ±1 dB may be achieved for omnidirectional hydrophones. Figure 3.8 shows a comparison of the response of a B&K8104 hydrophone calibrated by substitution using random noise with the free-field response.

The practical low frequency limit is usually the ability of the projector to generate a useful signal at low frequencies. At higher kilohertz frequencies, the results are sensitive to the exact positioning of the transducers (and the influence of the other transducers if simultaneous immersion is used). Another limitation is the influence of the directional response of the hydrophones. The hydrophones average the acoustic pressure across the surface of their elements, and since the acoustic waves are coming from many directions, the sensitivity measured is that averaged over all angular orientations - hence it differs from the free-field response to a plane-wave in a specified direction as described earlier. However, the field within the tank is unlikely to be perfectly diffuse, making it difficult to assess the discrepancy due to this effect. The effect on the calibration results can be minimised by using a reference hydrophone of the same type as the unknown hydrophone (the devices having similar

directional responses).

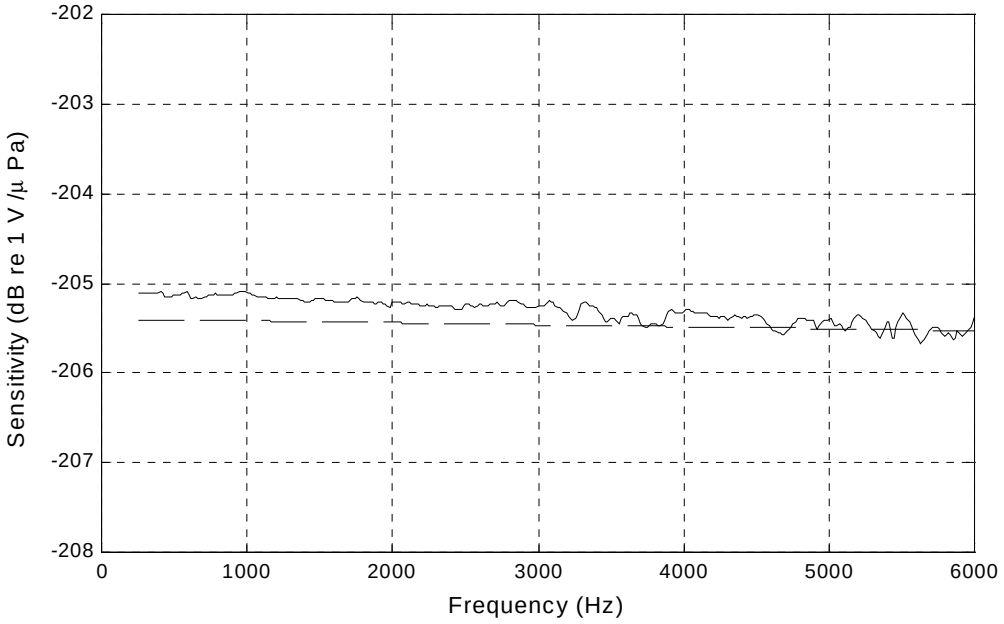

Figure 3.8 Calibration results for a B&K8104 hydrophone using the noise comparison method (smooth curve) plotted with the free field response (dashed line).

3.3 CALIBRATION USING A CROSS-CORRELATION TECHNIQUE

This method utilises broadband signals in a similar manner to the method described above, but attempts to eliminate the effect of echoes by use of windowing of the cross-correlation function. This method has been used extensively by DCN, France [4, 11, 12, 13].

3.3.1 Method

Remember that the cross correlation function, $\Gamma_{XY}(\tau)$, of the input signal *x(t)* and output signal *y(t)* is defined as;

$$\Gamma_{XY}(\tau) = \int_{-\infty}^{+\infty} x(t)\, y(t+\tau)\, dt \qquad (3.7)$$

where τ is a time delay. Since in this case the output signal is that obtained from the hydrophone, which in a reverberant tank is contaminated by echoes, the signal can be expressed as:

$$y(t) = \sum_{i=0}^{\infty} y_i(t - d_i / c) \qquad (3.8)$$

where c is the sound speed in water, $y_0(t)$ is the direct path signal with d_0 the separation between transducers, and $y_i(t)$ is an individual echo from the tank boundaries travelling a total distance d_i. Substituting for *y(t)* in the expression for $\Gamma_{XY}(\tau)$, we obtain:

$$\Gamma_{XY}(\tau) = \Gamma_{XY0}(\tau - d_0 / c) + \sum_{i-1}^{\infty} \Gamma_{XYi}(\tau - d_i / c) \qquad (3.9)$$

It can be seen that the cross correlation function is in fact the sum of the cross correlation

function of the input signal with the direct path signal arriving at time d_0/c, and the cross correlation of the input with the boundary echoes arriving at time d_1/c, d_2/c, etc. If the peaks in the cross correlation function $\Gamma_{XY}(\tau)$ are narrow enough, a window can be applied which selects only the direct signal and removes the boundary echoes which lie outside the window. From the windowed cross correlation function, the cross spectral density may be calculated according to:

$$\hat{G}_{XY}(f) = \Im\left\{\hat{\Gamma}_{XY}(\tau)\right\} \tag{3. 10}$$

where G_{XY} is the cross spectral density between the input and output signals, $\Im\{\}$denotes taking the Fourier transform and the ^ denotes that we are using the windowed function.

Note that an estimate of the transfer function, *H(f)*, of a system may be obtained from:

$$H(f) = \frac{G_{XY}}{G_{XX}} \tag{3. 11}$$

where G_{XX} is the power spectral density of the input signal and G_{XY} is the cross spectral density between the input and output signals. Since the transfer function in the case of a projector and hydrophone consists of the product of the individual transfer functions of the projector and receiving hydrophone, it is possible to derive the transfer function of the projector, S_P , from:

$$S_P = \frac{\hat{G}_{XY}(f)}{G_{XX}(f)\,M_R(f)\,H_W(f)} \tag{3. 12}$$

where M_R is the transfer function of the receiving hydrophone and H_W is the transfer function of the sound propagation through the water (for example an inverse dependence on distance for a spherically spreading acoustic field). When calibrating a hydrophone by comparison with a reference hydrophone and *keeping the separation distances for each hydrophone the same*, successive applications of the above equation for each device yields the following expression for the sensitivity, M_H , of the unknown hydrophone:

$$M_H(f) = \frac{\hat{G}_{XH}(f)}{\hat{G}_{XR}(f)}\,M_R(f) \tag{3. 13}$$

where the subscript *H* relates to the hydrophone under test, and the subscript *R* relates to the reference hydrophone.

If a window is to be successfully applied to the cross-correlation function, the function peak must be narrower than $(d_1-d_0)/c$ where d_1 is the distance travelled by the first echo. This requires the use of an input signal with a narrow peak in its autocorrelation function, which means that it must have a large bandwidth in the frequency domain. Thus a Gaussian random noise signal is an appropriate choice of signal. It should be noted that for the method to be successful, the coherence function must be close to unity by a similar argument to that in section 3.2.2. Another signal which has been used is a linearly frequency-modulated sine-wave [13]. Such a signal gives an excellent coherence function but produces slightly broader peaks in the cross-correlation function, making the windowing slightly more difficult.

3.3.2 Discussion

Many of the discussion points raised in Section 3.2 apply equally to this method

(considerations of coherence, etc). Using this method, DCN (France) have reported differences of less than 1 dB with the free-field calibration (measured in a lake) for an ITC1001 projector (Q-factor ≈ 3.5) in the range 500 Hz to 1.5 kHz. However, for higher-Q projectors, the transducer response narrows the bandwidth of the transmitted acoustic signal, which means that the peaks in the cross-correlation signal are broadened making it difficult to distinguish the peaks and therefore window out the reflections.

One solution to this is to pre-condition the drive signal in order to broaden the bandwidth of the signal emitted by the high-Q projector. Such an approach was adopted by Kashiwagi [14] who used a random signal which could take a value of +1 or -1 with the time intervals between each change of state following a Poisson distribution. This can be made to provide a drive signal spectrum with two peaks placed either side of the transducer resonance peak, the resultant acoustic spectrum being a broadened version of that produced by the transducer driven by noise of a Gaussian distribution. DCN have implemented this technique and reported improved results for high-Q projectors [4, 13].

3.4 HOMOMORPHIC SIGNAL PROCESSING (CEPSTRAL DECONVOLUTION)

This method is analogous to that of Section 3.3 in that a form of deconvolution is involved, but the windowing or filtering is undertaken in the complex cepstrum domain [15]. This type of processing is sometimes termed homomorphic signal processing and has been used for the removal of the effect of the transmission path (for example, the effect of echoes) from signals in a number of fields such as seismology [16] and audio signal processing [17].

3.4.1 Method

The complex cepstrum is defined as the "inverse Fourier transform of the complex logarithm of the complex spectrum (the forward Fourier transform of the time domain signal)" [18]. In terms of a mathematical formula, the cepstrum $C(\tau)$, of time-domain signal s(t) is given by:

$$C(\tau) = \Im^{-1}\{\ln(\Im\{s(t)\})\} \quad (3.14)$$

where ln denotes taking the complex natural logarithm and $\Im\{\}$denotes taking the Fourier transform. The independent variable of the resulting signal has been termed "quefrency" [15] though it has the dimensions of time and is similar to the "τ" of the autocorrelation function. If the spectrum is expressed as $A(f)\exp(i\phi(t))$, the complex logarithm is given by:

$$\ln[A(f)\exp(i\phi(f)] = \ln[A(f)] + i\phi(f) \quad (3.15)$$

The cepstrum of a signal has several properties which make it useful. Firstly, the parts of the spectrum which vary only slowly (which are typical of a smooth transfer function) are gathered around the origin in the cepstral domain, whereas any rapid spectral variations (for example those caused by interfering echoes) are not moved. Secondly, due to the effect of taking logarithms, signals which are multiplied in the spectrum are summed in the cepstrum, which means that signals convolved in the original time domain signal will be summed in the cepstrum also [19, 20]. Note that the phase function must be made continuous (unwrapped as opposed to modulo 2π) if the logarithm is to have the property that multiplications in the frequency spectrum are to transform to additions after the logarithm is taken.

The above properties allow convolved effects in time signals to not only be separated in the cepstrum, but it is possible to remove an unwanted effect completely and return to the original time signal without this effect. For example, the effect of a signal transmission path can be negated by subtracting the cepstrum of its transfer function in the cepstral domain from the cepstrum of the measured signal [21].

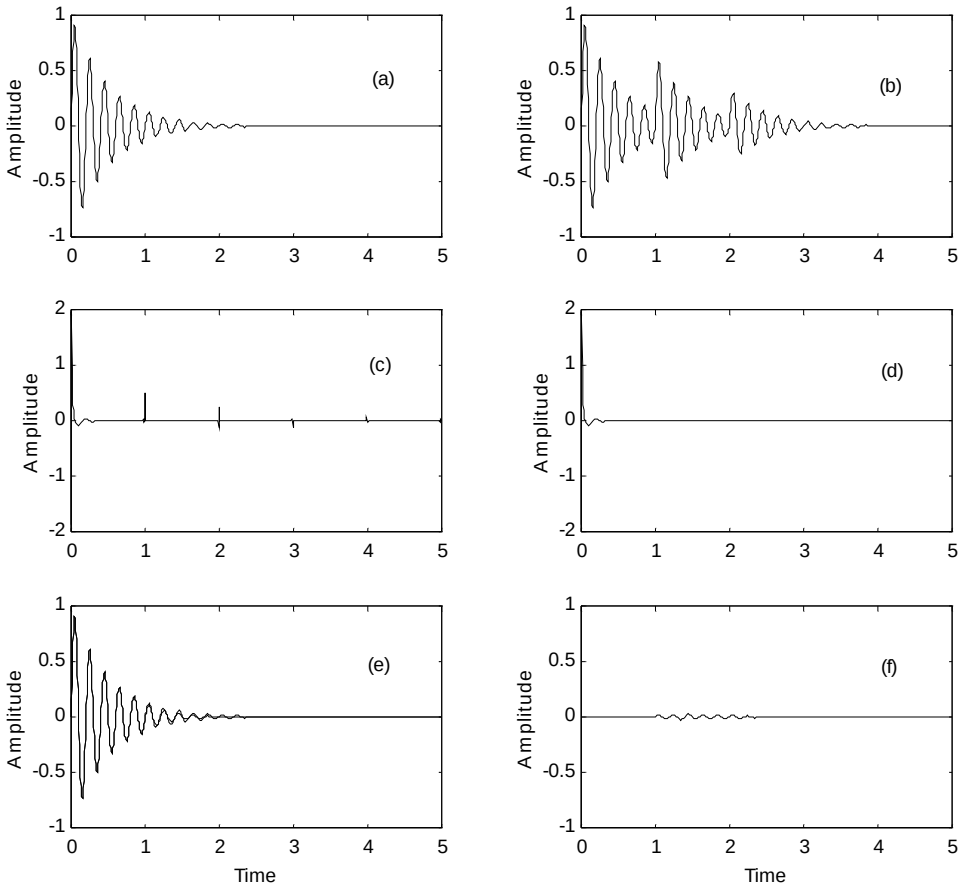

Figure 3.9 Illustration of echo removal using the complex cepstrum: (a) source signal; (b) source signal with two echoes; (c) complex cepstrum of signal with echoes; (d) filtered cepstrum; (e) reconstructed signal without echoes; (f) residual differences between reconstruction and original.

With more complex signals than those shown Figure 3.9, it can be difficult to subtract the contribution of the echoes to the cepstrum without some prior knowledge of what they are. Simple filtering does not always produce good results with convolutions of narrow-band signals since their cepstrum contributions are distributed. Improvements may be obtained by use of knowledge of the geometry of the acoustic test tank. If a broadband signal is used, the cepstrum shows a very narrow peak which allows the identification and removal of echoes by simple filtering [20].

3.5 MAXIMUM LENGTH SEQUENCES

Another random signal sometimes used in acoustic calibration is Maximum Length Sequences (MLS). An MLS is a pseudo-random distribution of binary values (zeros and ones) which if plotted looks essentially like a square-wave. The degree of the MLS is N where there are 2^N samples in the sequence. The MLS has a number of useful properties:

- the spectrum is broadband with magnitude equal to 2^N;
- the autocorrelation is a Dirac delta function around the origin with amplitude 2^N;
- the impulse response, *h(t)*, of a linear system subjected to an MLS is:

$$h(t) = \frac{\Gamma_{XY}(\tau)}{2^N} \tag{3. 16}$$

where $\Gamma_{XY}(\tau)$ is the cross-correlation function. For the binary MLS, the cross-correlation function may be calculated in essentially real-time by use of a fast Hadamard transform.

Once the cross-correlation has been calculated, the windowing methods described in earlier sections may be adopted. Such methods have been applied to airborne acoustic calibrations, and, when combined with homomorphic signal processing, to the calibration of low frequency projectors in reverberant tanks [20].

3.6 CALIBRATION FROM NOISE POWER MEASUREMENTS

3.6.1 Method

The transmitting response of a projecting transducer is defined as the acoustic pressure generated at a point a known distance from the source and in a given direction for a known electrical stimulation. For a spherical-wave field, the pressure varies inversely with distance, *r*, so that the product of the acoustic pressure and the propagation distance ($P\,r$) is a measure of the strength of the source (in Pa m), and is the parameter we need to measure to determine the transmitting response (along with the drive current or drive voltage). This parameter may be estimated from a measurement of acoustic power.

Consider the total acoustic power for a spherical-wave source. The total acoustic power, *W*, for a spherically-divergent wave is given by the average rate at which acoustic energy flows through a closed spherical surface of radius *r*, leading to [7]:

$$W = 4\pi r^2 I = 4\pi r^2 \frac{P^2}{\rho_0 c} = \frac{4\pi}{\rho_0 c}(P\,r)^2 \tag{3. 17}$$

which is an expression for acoustic power in terms of the quantity $P\,r$ which determines the transmitting response, and where *I* is the acoustic intensity and ρ_0 is the water density and *c* is the sound speed. Hence, a measurement of acoustic power can be used to derive a value for $P\,r$.

One way to measure the acoustic power is to use a reverberant environment (a reverberation chamber or reverberant tank) [6, 7]. In a reverberant field, the total acoustic pressure, P_T, may be obtained from the sum of the contributions of the direct and reverberant field (see

Appendix B) and expressed as:

$$P_T^2 = W\rho_0 c\left[\frac{1}{4\pi r^2} + \frac{4}{A}\right] \quad (3.18)$$

where A is the total absorption of the enclosure. If the expression for the acoustic power is substituted into the above expression, we obtain:

$$P_T^2 = (Pr)^2\left[\frac{1}{r^2} + \frac{16\pi}{A}\right] \quad (3.19)$$

Assuming a measurement of the drive signal is also available, this expression may be used to derive a calibration of a projector. If the square of the total acoustic pressure is plotted against the reciprocal of the square of the separation distance, the results should be a straight line, the square root of the gradient providing an estimate of Pr. The acoustic pressure may be obtained by use of a small omnidirectional calibrated hydrophone.

Note that the intercept also depends upon the total acoustic power. Since at a sufficient distance away from the source the reverberant field will dominate (and is constant and independent of position), a calibrated hydrophone may simply be positioned there to provide a measurement of the power (and a calibration of the projector). However, since the fields in underwater tanks are not highly reverberant, this provides only a crude calibration, better accuracy being obtained by use of the direct field as well and deriving the response from the gradient of a straight line fit.

Although primarily intended for the measurement of radiated power from noise sources (eg a Remotely Operated Vehicle (ROV)) in reverberant acoustic tanks [22, 23], such techniques have also been used to derive the transmitting response of a projector with Gaussian random noise used as the drive signal [24, 25].

3.6.2 Results

Measurements have been attempted by NPL using an ITC1001 projector driven by a Gaussian noise source amplified through a 100 W power amplifier. The measurements were made in a 5 x 4 x 4 m steel-walled water tank located at Sonardyne International Ltd. A calibrated hydrophone (Reson TC4034) was used to measure the resulting acoustic pressure field at a number of known projector-hydrophone separation distances. The spectrum of the acoustic signal measured by the hydrophone was captured using a signal analyser and stored for further analysis. A simultaneous measurement was made of the spectrum of the drive voltage applied to the projector.

Using the frequency response curve for the calibrated hydrophone, the hydrophone voltage spectrum was converted to acoustic pressure and then squared. For each separation distance, the corresponding pressure squared spectrum was averaged in a frequency band around a specified centre frequency, and the value of the product of pressure and separation distance was determined from the square root of the gradient of the graph of P_T^2 versus $1/r^2$. This process was repeated for centre frequencies in the range 5 kHz to 30 kHz.

A similar analysis was applied to the drive voltage spectra (using the identical range of centre frequencies and averaging bandwidth) to provide a drive voltage versus frequency curve which was then used to calculate the Transmitting Voltage Response (TVR) in dB re 1 μPa m/V. The analysis was undertaken automatically using routines written in the Matlab programming language. An averaging bandwidth of 2 kHz was used initially, but this value was varied to determine the sensitivity of the analysis results to the size of the averaging bandwidth.

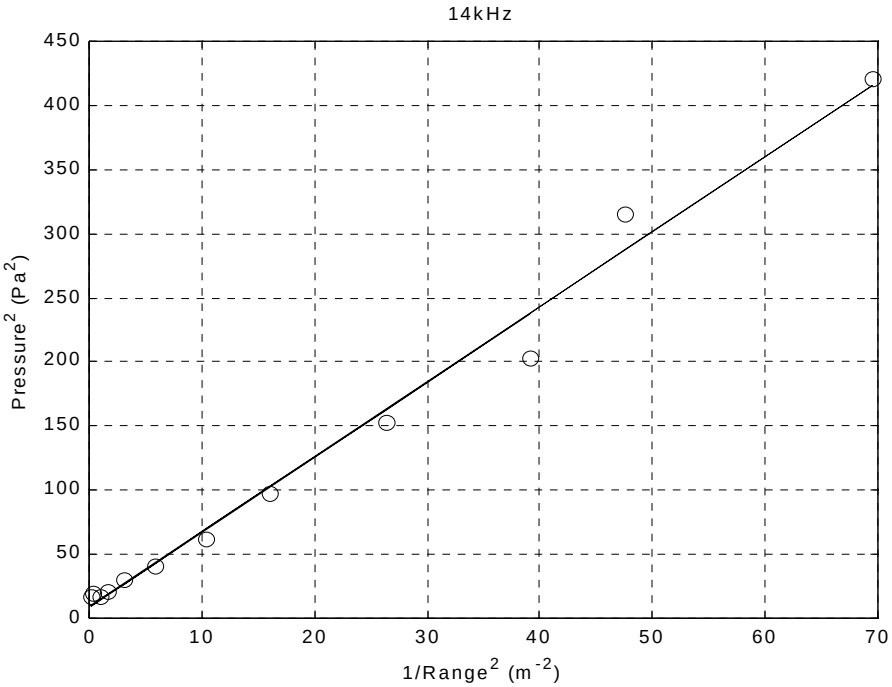

Figure 3.10 An example of a plot of P_T^2 versus $1/r^2$ for a centre frequency of 14 kHz and an averaging bandwidth of 2 kHz showing least-squares fitted straight line and data points (o).

Figure 3.10 shows an example of the straight line fit for spectral data averaged in a bandwidth of 2 kHz around a centre frequency of 14 kHz. This is a typical example of the measurement data. Figure 3.11 shows a comparison of the results of this calibration for the ITC1001 projector with those obtained from a free-field calibration. As can be seen, the agreement is within about 1 dB in the range 10-30 kHz. However, measurements on other projectors have shown differences of typically up to 2 dB from the free-field value.

3.6.3 Discussion

As with some of the other reverberant methods described here, one would expect the results of a calibration performed in a reverberant field to differ from the free-field value by the directivity factor. If the measurements are performed using the direct field (as shown in the plots here), the situation is a little more complicated since the direct field is dominating for measurements close to the projector. It is therefore preferable to keep the same orientation between the hydrophone and projector during the measurements. If the tank used for the calibrations is not very reverberant, the first reflection arriving will tend to dominate and the

reverberant field will not be constant with position. This means that the straight line plots will show much more structure and this in turn will show up as perturbations on the TVR plots. The averaging bandwidth used must also be optimally chosen - too narrow and not enough smoothing occurs, too broad and genuine features in the underlying response may be smoothed out.

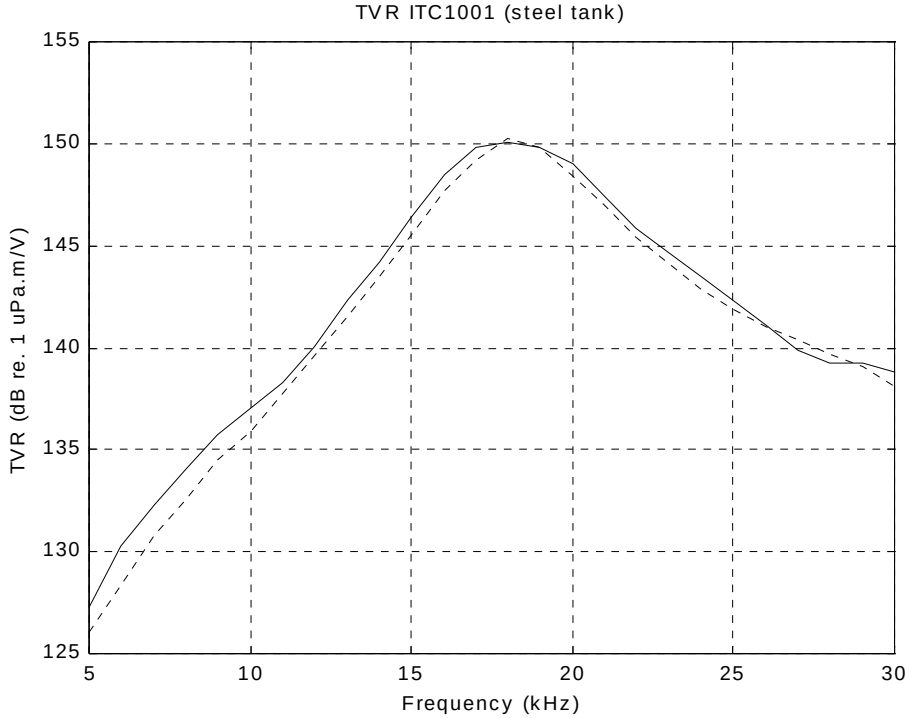

Figure 3.11 Comparison of the TVR for an ITC1001 derived from noise power measurements (smooth line) and from free-field calibrations (dashed line).

3.7 TIME DELAYED SPECTROMETRY

The method of time delayed spectrometry (TDS) has been used for calibration of transducers in both airborne acoustics [26] ultrasonics [27], and underwater acoustics [4]. In TDS, a projector is driven with a sinusoidal signal, *V(t)*, the frequency of which is swept over the frequency range of the calibration such that:

$$V(t) \quad = \quad A\cos[\,2\pi(\,f_m - S\,t\,)\,t\,] \tag{3. 20}$$

where A is the signal amplitude and f_m is the maximum frequency and S is the sweep rate or rate of change of frequency with time (= df/dt). The signal received by the hydrophone consists of the direct path signal plus reflected signals from the tank boundaries. Since the reflected signals arrive later in time than the direct path, they will be at a different frequency and so may be removed by use of a narrow-band filter. The centre frequency of the filter must be made to track the direct-path signal by being swept at the same rate as the drive signal to the projector. The experimental arrangement to allow such a measurement to be made can be achieved by use of a swept spectrum analyser where the tracking filter can be offset in frequency from the output of the oscillator.

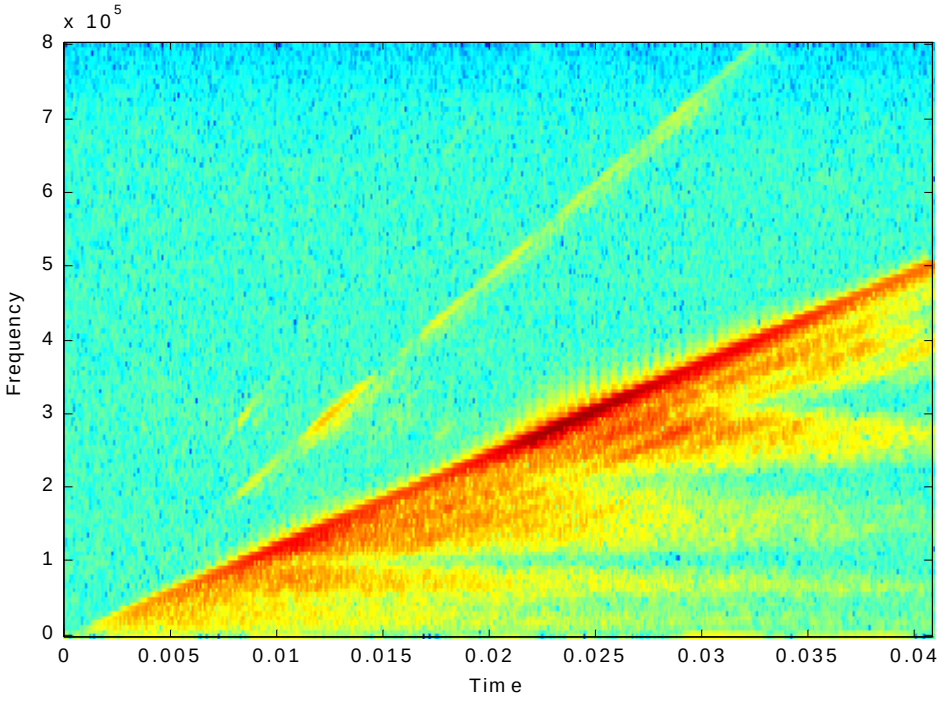

Figure 3.12 An example of a spectrogram (FFT versus time) plot of the unfiltered digitised receive signal from a TDS experiment where the frequency was swept from 10 to 500 kHz. The colours represent normalised amplitude (red: highest; dark blue: lowest). Frequency is in hertz, time in seconds.

Another possible way to conduct the experiment is to digitise the unfiltered receive signal and store for processing later. Digital signal processing (eg a digital filter) may then be used to extract the amplitude of the signal at the appropriate frequency. This approach has some significant disadvantages over using a real-time analyser since more processing is required and large record lengths must be stored. However, it is useful to illustrate the method. Figure 3.12 shows an example of a spectrogram (FFT amplitude versus time plot) of a signal recorded by a hydrophone when the projector is driven with a continuous sinusoidal waveform which has been swept from 10 to 500 kHz. The processing here involved scanning a 256-point FFT window through the 65 k long time waveform and plotting the FFT amplitudes versus time, with the amplitudes represented here using an arbitrary colour coding. In the plot, the reflections are clearly visible arriving after the direct signal at any given frequency.

This method offers good signal to noise performance and the potential for fine-frequency resolution. However, it requires the use of appropriate signal analysers (not always available) and broadband projectors which can produce acceptable signal levels at a range of frequencies and which do not generate severe start-up transients. Fine-frequency resolution can be obtained, but only at the expense of the ability to distinguish between different propagation paths.

3.8 MODELLING THE ACOUSTIC FIELD IN THE TANK

If a suitable model for the test tank can be constructed, it may then be possible derive the response of the source (ie the projector under test) from measurements of the acoustic pressure in the tank by working "backwards".

A number of methods of modelling an acoustic field in a reverberant enclosure are in common usage. These might be regarded as belonging to several broad classes:

- (semi) empirical methods

- the many rules and formulæ in use in classical acoustics (eg Sabine's and Eyring's);

- geometrical methods

- these include ray tracing, method of images, etc;

- numerical methods
  - finite elements and boundary elements.

Some further information on each of the principles behind each of the above methods is given in Appendix C.

Some methods based on the classical room acoustics formulæ have already been touched upon in Section 3.6 [23,24,25]. Ray tracing methods have been more extensively applied to the acoustics of air-filled rooms [28] rather than underwater acoustic test tanks, although in principle these could be applied at higher frequencies where wave phenomena can be neglected.

The most useful of the above approaches for the calibration of underwater acoustic transducers at frequencies of a few kilohertz is that of finite element and boundary elements. With such methods, it should be possible to completely describe the field inside the measurement tank due to the source projector. Attempts to do this have been reported for enclosed sources in both air [29,30,31] and water [32,33]. There are a number of problems and limitations with such modelling approaches when applied to calibrations in test tanks:

- as an input to the model, accurate knowledge of the acoustic properties of the tank is often required. Ideally, the acoustic properties (eg reflection coefficient) of all of the boundaries must be known as a function of frequency (and angle of incidence). Since such data is not readily available (and difficult and time consuming to measure), this imposes limits on the model accuracy. This applies to both FE/BE and ray tracing models.

- to obtain sufficient accuracy may require large model sizes, with obvious implications for time and computing expense. Large FE mesh sizes may be required to completely model a tank including boundaries at the required spatial sampling rate (for ray tracing, many images may be required).

- in FE/BE models, if a range of frequencies are to be investigated, the model may have to be re-meshed to accommodate the different frequencies.

- with tanks made from solid walls rigidly connected to the ground, the potential exists for the sound to exit through the walls and propagate in the surrounding medium, perhaps re-entering through an alternative boundary. Inclusion of such effects into the model would be very difficult.

- perhaps the biggest disadvantage is that any model is time-consuming to construct and has to be tailored to the particular tank (and maybe the particular transducer) under investigation. This limits the application of the model to specific examples and militates against its general applicability.

Since the development of such models is not by any means a trivial task and certainly not to be attempted lightly, it is perhaps only an option for specialised measurement tanks where other larger volumes of water are not readily available as an alternative measuring environment, for example in the case of an anechoic pressure vessel [34].

4. METHODS MAKING USE OF THE ECHO-FREE SIGNAL

4.1 EXTRAPOLATION USING SIGNAL MODELLING

4.1.1 Background

Figure 4.1 shows an example of a waveform detected by a hydrophone for a moderately high-*Q* transducer driven at its resonance frequency. Clearly, the steady-state is not reached in the available time-windows indicated in the plot. For example, in the 5.5 m diameter by 5 m deep measurement tank at NPL, the echo-free time of about 2.5 ms allows 5 cycles of 2 kHz signal. For even a moderately resonant transducer (say *Q*-factor = 10), the steady-state cannot be observed and all the methods described in Section 2.3 will fail.

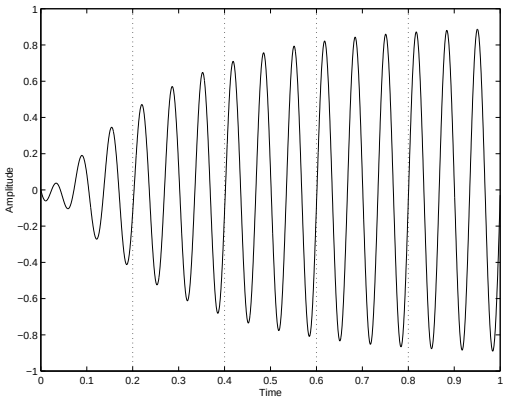

Figure 4.1 An example of a normalised waveform for a moderately high-*Q* transducer driven at its resonance frequency. Note that steady-state is not reached within the available time windows indicated.

These difficulties may be at least partly overcome if greater use can be made of the initial transient-dominated part of the waveform, in particular if the steady-state signal can be predicted by fitting a model to the initial transient-dominated data. This motivates the work summarised in this section. This approach has been attempted by a number of laboratories in the field such as USRD-NRL in the USA [35, 36]. In the description given here, the detail is based on the work at NPL [37, 38].

4.1.2 Signal models

If we consider the response of an electroacoustic transducer at frequencies at or below its first resonance frequency, it is reasonable to assume the behaviour is that of a damped harmonic oscillator. This corresponds to the regime where the device may be modelled with a so-called “lumped-parameter” model. The behaviour of a damped harmonic oscillator is governed by a linear constant coefficient differential equation of the kind familiar from the analysis of systems of masses, springs and dampers (or in an electrical analogue, a resonant LCR circuit). The solutions of such a differential equation are also well known to be combinations of damped sinusoids or, expressed in an alternative way, as a sum of complex exponentials.

In order to achieve good *prediction* from the model fitted to the data (which is important when direct measurement of the steady-state is limited), it is necessary to consider *physical* models. We assume that the measured signal $y(t)$ corresponds to the output of a system that behaves as a linear damped harmonic oscillator, and consequently $y(t)$ solves a linear constant coefficient differential equation of the form

$$\sum_{k=1}^{p+1} c_k \frac{d^{k-1}}{dt^{k-1}} y(t) = 0. \qquad (4.1)$$

Solutions to this differential equation include damped and undamped sinusoids and real exponential functions. With appropriate initial conditions, equation 4.1 defines completely the output $y(t)$. A model for $y(t)$ may be derived using solutions to equation 4.1. Using *a priori* knowledge about $y(t)$, this model may be written in the particular form

$$y(t) = A_0 \sin\{2\pi f_0 t + \phi_0\} + \sum_{k=1}^{n_r} A_k e^{d_k t} \sin\{2\pi f_k t + \phi_k\}, \qquad (4.2)$$

where the first term is used to describe the steady-state behaviour of the device, and the remaining terms its resonant behaviour. The solution to equation 4.1 is also given by

$$y(t) = \sum_{k=1}^{p} \alpha_k e^{\beta_k t}. \qquad (4.3)$$

Equation 4.3 defines the *complex exponential* parametrisation for the output $y(t)$. The variables β_k, $k = 1, \ldots, p$, are known as *poles*, and are the roots of the characteristic polynomial defined by $\{c_k\}$. The variables α_k, $k = 1, \ldots, p$, are known as *residues*, and are determined by the initial conditions for $y(t)$. Notice that the parameters in this model are divided into those (the residues) that appear *linearly* in the model, and those (the poles) that appear *nonlinearly*. This has important implications for algorithms for fitting the model to measured data.

4.1.3 Fitting the model to the data

The models of this form are fitted to data $\{(t_i, y_i): i = 1, \ldots, m\}$ measured at equally spaced times t_i. If ε_i is the measurement error for the ith data value y_i, and the values t_i are known accurately, the function $y(t)$ satisfies the *observation equations*

$$y_i = y(t_i) + \varepsilon_i, \qquad i = 1, \ldots, m. \qquad (4.4)$$

Assuming the errors ε_i are uncorrelated samples from a Gaussian probability distribution with mean zero and standard deviation σ, unbiased and efficient estimates of the parameters defining $y(t)$ are obtained by solving

$$\text{minimise} \quad \sum_{i=1}^{m} \{y_i - y(t_i)\}^2 \tag{4.5}$$

with respect to the parameters of $y(t)$. The residuals $e_i = y_i - y(t_i)$ evaluated at the solution provide estimates of the errors ε_i, and an estimate of σ is given by the root-mean-square error s where

$$s = \sqrt{\frac{1}{m-n} \sum_{i=1}^{m} e_i^2}, \tag{4.6}$$

and n is the number of parameters defining $y(t)$.

If *a priori* knowledge of any of the model parameters is available, this information can be represented by additional observation equations, and the estimation problem is modified accordingly. For example, if f_r and d_r are the frequency and damping factor for a resonance of the system, the estimation problem becomes

$$\text{minimise} \quad \sum_{i=1}^{m} \{y_i - y(t_i)\}^2 + u^2 \{f_r - f_1\}^2 + v^2 \{d_r - d_1\}^2, \tag{4.7}$$

where u and v are "weights" that are used to reflect the relative accuracy between the measured data and the *a priori* knowledge.

Since the signal *model* is not linear (it is composed of exponential functions), the fit is performed by use of a nonlinear least squares algorithm to achieve a best fit in a maximum-likelihood sense (section 4.1.5). This has significant advantages over linear estimators such as the classic method of Prony (section 4.1.4). However, since a reasonable initial estimate is required for the nonlinear least squares method to be accurate, a modified form of Prony's method has been used to provide this.

4.1.4 Linear estimation methods

Linear estimation methods are based on the observation that the model values $y(t_i)$ satisfy a set of recurrence equations, with undetermined parameters $\delta_1, \delta_2, \ldots, \delta_{p+1}$:

$$\delta_1 y(t_i) + \delta_2 y(t_{i+1}) + \ldots + \delta_{p+1} y(t_{i+p}) = 0, \qquad i = 1, \ldots, m - p. \tag{4.8}$$

Replacing the values $y(t_i)$ by the measured values y_i, the recurrence equations are no longer satisfied exactly, but instead

$$\delta_1 y_i + \delta_2 y_{i+1} + \ldots + \delta_{p+1} y_{i+p} = e_i, \qquad i = 1, \ldots, m - p. \tag{4.9}$$

Figure 4.2 illustrates the way the recurrence equations are formed for the case $p = 4$ (four poles and residues defining two sinusoidal components) and a data set composed of 21

equispaced samples (m = 21). The numbers beside a data sample indicate the use of that sample within particular recurrence equations. For example, the first data sample appears in the first recurrence equation, the second data sample appears in the first and second recurrence equations, and the third data sample is used in the first three recurrence equations. In total there are $m - p = 17$ recurrence equations to be solved for $p + 1 = 5$ Prony parameters δ_i.

The equations 4.9 constitute a set of linear equations for the parameters $\delta_1, \delta_2, \ldots, \delta_{p+1}$. If we set $\delta_{p+1} = 1$ (note the parameters are determined up to a scale factor), we determine estimates of the parameters $\mathbf{d} = (\delta_1, \delta_2, \ldots, \delta_p)^{\mathrm{T}}$ by solving the least-squares problem

$$\text{minimise} \quad \boldsymbol{e}^{\mathrm{T}}\boldsymbol{e}, \qquad \boldsymbol{e}^{\mathrm{T}}\boldsymbol{e} = \sum_{i=1}^{m-p} e_i^2, \tag{4.10}$$

with respect to **d**. The poles β_k for the system are then recovered from the parameters $\delta_1, \delta_2, \ldots, \delta_{p+1}$. Finally, the residues α_k are obtained by fitting the model of equation 4.3, now regarded as a function of α_k only, to the data: this is another linear least-squares problem.

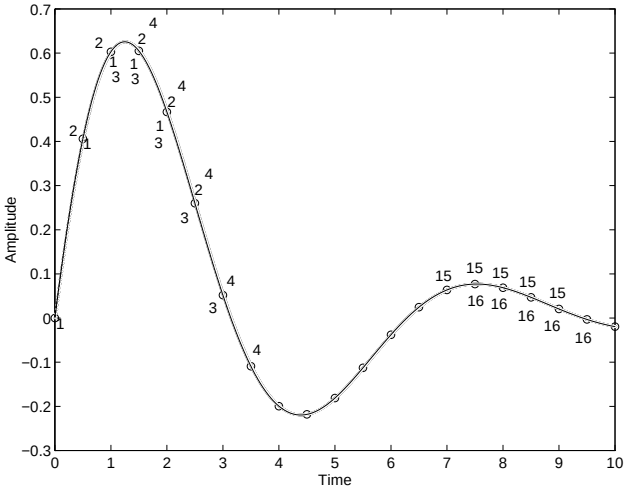

Figure 4.2: Formation of the recurrence equations in the application of the least-squares Prony method for the case p = 4 and m = 21.

The procedure described above is the *least-squares Prony method* described in [35, 39, 40, 41]. It is noted in [42] that although the method is consistent as $\sigma \to 0$, it is inconsistent as $m \to \infty$. (In other words, in the presence of noise, the method gives estimates that do not converge to the true solution as the number of sampled points increases.) Consequently, the method is only useful for low noise levels regardless of how many measurements are made. This has led to the development of a number of variations on the basic method, as follows:

a) The *modified least-squares Prony method* in which, instead of adjacent samples, every lth sample is used to satisfy the recurrence equations [35].

b) The use of a large number *p* of poles with *forward* and *backward prediction* to help in distinguishing between "true" system poles and poles associated with measurement noise [39].

c) The *Prony-SVD* method in which a large number *p* of poles is used with the singular value decomposition [43]. (An alternative to the singular value decomposition is to use complete orthogonal factorization [36].)

d) A *weighted* version of the least-squares Prony method that correctly accounts for the error structure in the original measured data [37, 38].

There has also been work concerned with including *a priori* information. In [39], this is done by applying a filter to the data to remove known system poles before applying a Prony method; in [36, 44], recurrence equations relating samples of the input *and* output signals are used to model the system's transfer function.

4.1.5 Nonlinear estimation methods

The estimation problems defined by equations 4.5 and 4.7 are nonlinear least-squares problems. Standard algorithms exist (see, for example, [45]) for solving this type of problem including the Gauss-Newton and full-Newton methods. These are iterative methods that at each iteration take a step towards the minimum by solving a linear least-squares problem. The algorithms differ in the amount of information that needs to be supplied about the model: the Gauss-Newton method requires that the first derivatives of the model with respect to its parameters are available, whereas in a full-Newton method the second derivatives are also required.

In addition to choosing an algorithm specific to least-squares problems, it is possible to exploit structure in the model. The parameters naturally separate into those (the poles or equivalently frequencies and damping factors) that appear nonlinearly in the model, and those (the residues or equivalently amplitudes and phases) that appear linearly. The use of variable projection methods as described in [36] exploits this structure in the solution of the nonlinear least-squares problem. Yet another approach is presented in [42], involving a reparametrisation of the model and the solution of a nonlinear eigenvalue problem.

It is usual to use the solution from a linear prediction method to provide starting estimates for solving the nonlinear estimation problem. In [37, 38] it is noted that in order to obtain good fits using linear prediction methods, it may be necessary to choose a model for which the number of damped sinusoidal components exceeds what is believed to be the number of "true" resonances. It is also illustrated that the nonlinear estimation problem defined by equation 4.5 is inherently ill-conditioned, i.e., large changes in the frequency and damping factor parameters may produce small changes in the residual sum of squares function that we wish to minimise. These facts can make it difficult for standard algorithms to converge satisfactorily to a solution.

The method described in [37, 38] uses a Gauss-Newton algorithm, safe-guarded with a line search algorithm with *a priori* information incorporated as described in section 4.1.3, equation 4.7. Furthermore, if additional damped sinusoidal components are used to define the initial model fit, these are either explicitly removed prior to applying the Gauss-Newton algorithm or *regularisation* is used to replace the estimation problem to be solved by one that is better conditioned.

4.1.6 Results

Presented in Figure 4.3 are estimates of the transmission voltage response for an ITC1001 projector calculated using a calibrated hydrophone where, at each frequency, the voltage output of the hydrophone is estimated using the modelling method described above. The free-field transmission voltage response is shown using “small circles”. The transmission voltage responses obtained by analysing data contained within the time-windows comprising (a) 3 cycles and (b) 1.5 cycles of the resonance frequency are shown as, respectively, a solid line and a dashed line.

In each case and for each frequency, the decision to accept an estimate of the steady-state response was made as objective as possible. The decision was based on how well the data within the time-window considered was fitted. A fitted model was only accepted if it satisfied the convergence criteria implemented for the nonlinear estimation problem, and wherever possible, a model was chosen to reflect the belief that only one resonance is present in the system.

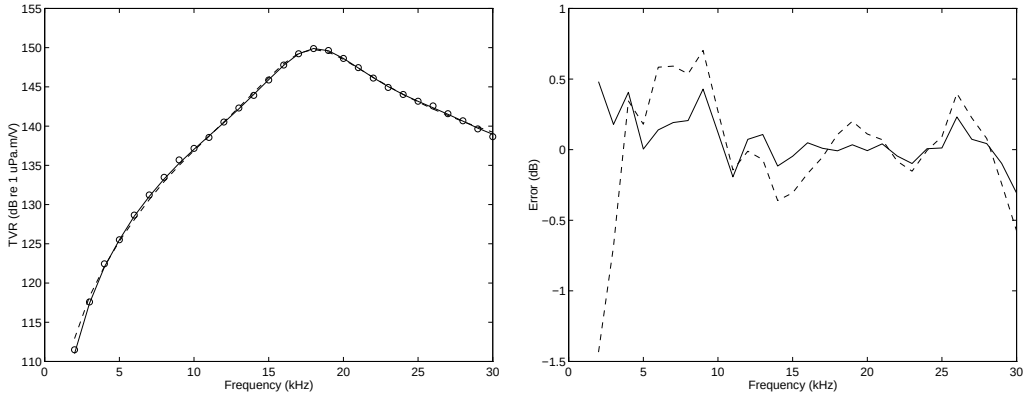

Figure 4.3 On the left, transmission voltage responses from (i) free field measurements (small circles), (ii) measurements from a time-window comprising 3 cycles (solid line), and (iii) 1.5 cycles (dashed line) of the resonance. On the right, the differences between (i) and (ii) (solid line), and between (i) and (iii) (dashed line).

Results indicate that for moderately resonant transducers, errors of less than 1 dB will result if approximately one cycle of the resonance frequency is available is used in the analysis. For the example of the measurement tank at NPL, it can be seen that transducers with resonance frequencies as low as 400 Hz may be calibrated with acceptable accuracy.

4.1.6 Discussion

This method is particularly suited to use in the testing of projectors, but may be used in the calibration of hydrophones and in the measurement of directional response or even in the determination of the acoustic properties of materials from panel measurements. As indicated in the above sections, there are some technical difficulties which must be addressed when implementing the method. These include:

- selection of the model order (number of poles);
- distinguishing between signal poles and noise poles;
- sensitivity to artefacts introduced experimentally, such as DC bias;
- sensitivity to model accuracy or appropriateness;
- sensitivity to time window selection (to start at the beginning of the signal and include no reflections);
- computational efficiency, automation and interface with routine calibration software.

The method described here becomes progressively less accurate as the data becomes more noisy, and also as the *Q* of the transducer is increased since the available information about the damping factor of the resonance in a given time-window is reduced. With very short time-windows and higher-Q devices, the independence of the basis functions used to form the model is reduced, especially for driving frequencies close to resonance where it can be difficult to distinguish the drive signal from the natural response [46]. DC bias can be removed from the signal prior to modelling (or added as an extra term) and the techniques described in Section 4.1.4 can be successfully used to reduce sensitivity to noise, but these are not perfect. The model assumed here is a so-called “lumped parameter” model assuming a point projector. Modelling an extended projector using a small number of poles and zeros is not really valid.

To help overcome some of these problems for high-Q projectors, Ainsleigh and George have extended the method to include terms to represent the first few echoes from the tank walls, the extra terms having suitable time-delays, amplitudes and phases. This has worked well for the calibration of flexural disc transducers with a Q as high as 12, but it was found that the model estimates were very sensitive to errors in the estimates of the echo arrival times [36].

4.2 DERIVING TRANSDUCER RESPONSE FROM SIMPLE MODELS

The simple lumped parameter models discussed in the last section can be used to estimate the entire frequency response of the transducer under test. In practice, it can easily be arranged for the poles due to the measurement system to be at considerably different frequencies to that of the projector resonance frequency (by use of small hydrophone receiver, wideband amplifiers, no narrowband filters, etc). In such a case, the resonance behaviour observed in the data and reflected in the fitted model will be that solely due to the projector. An estimate of the resonant behaviour of the projector is then obtained directly from the model parameters derived from the methods of Section 4.1, and these can be used to predict the response over a range of frequencies.

A convenient analogy is to suppose that the projector may be modelled using an equivalent electrical circuit composed of a blocked capacitance in parallel with an LCR-circuit. The blocked capacitance is used to represent the electrical behaviour of the device at low frequencies, whereas the LCR-circuit represents its mechanical and acoustic properties when driven near to its resonance. Furthermore, it may be assumed that the pressure waveform generated by the device is a scaled replica of the motional current flowing through the LCR-circuit. The choice to use this particular equivalent circuit is because *if* the current and pressure are directly coupled as described, the choice is consistent with the models used to represent the measured signals $y(t)$ in equation 4.2. An illustration of such a circuit is given in Figure 4.4.

Now, given estimates for the resonance damping factor d and resonance frequency f for the device (for example from the methods of Section 4.1), an analysis of the circuit in Figure 4.4 may be made to determine the relative sizes of the circuit elements L, C and R. The amplitude transmitting voltage response of the projector, S_P, as a function of the drive frequency ω_0, may then be determined from [38]:

$$S_P = \frac{Kd}{L} \frac{\omega_0}{\sqrt{((\omega^*)^2 - \omega_0^2)^2 + \omega_0^2 (R/L)^2}}, \quad \omega^* = \sqrt{\frac{1}{LC}}, \tag{4.11}$$

where K is a scaling factor. The function is completely defined by d and f (which determine R/L and $1/LC$), *and* by the value of S_P at a single frequency (which determines the factor Kd/L) [38]. Furthermore, these three pieces of information may be obtained from an analysis of the measured signal $y(t)$ at a *single* frequency.

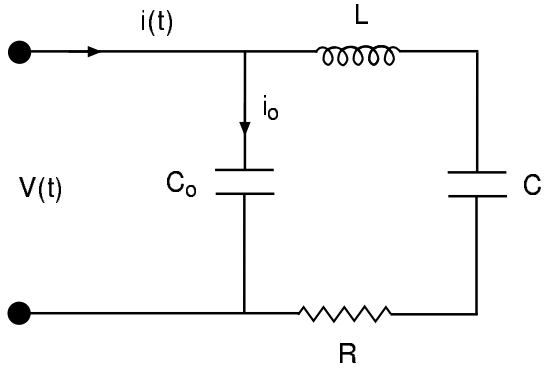

Figure 4.4 An example of an equivalent circuit for a spherical piezoelectric transducer showing circuit elements for the electrical and motional impedance where C_0 is the blocked capacitance, L, C and R represent the motional impedance.

In Figure 4.5 estimates are presented of the transmitting voltage response for the ITC1001 projector calculated using equation 4.11 and estimates of the resonant behaviour of the device. For comparison, the (free-field) transmitting voltage response is included (defined by the "small circles" in the figure). Four curves are shown corresponding to estimates of the resonant behaviour obtained by processing the data corresponding to the following drive frequencies: 10 kHz, 18 kHz, 20 kHz and 30 kHz. The data analysed was contained within a

time-window comprising 3 cycles of resonance frequency. The transmitting voltage response is expressed in (linear) units of Pa m/V (on the left) as well as in units of dB re 1 μPa m/V (on the right).

Note that the curves shown in Figure 4.5 are obtained by evaluating a *model* for the transmitting voltage response defined by parameters that depend on estimates of the resonant behaviour. Note that each curve in these figures is generated *completely* from the analysis of data corresponding to a *single* drive frequency. However, the estimates of the transmitting voltage response generated in this way are less satisfactory than evaluating the response at each frequency by extrapolation (as is done in Section 4.1), in particular for low frequencies. The reasons for this may be that (a) the model of the transmitting voltage response is deficient (because the equivalent electrical circuit from which the model is derived is too simple), and (b) the estimates of the resonant behaviour are not sufficiently accurate. Certainly, the estimated model obtained from measurements made at the lowest frequency of 10 kHz are the least accurate, and this is where the data is hardest to model. Furthermore, as is described in the discussion of the conditioning of the estimation problem (Section 4.1), obtaining estimates of the resonant behaviour is more difficult than estimating the steady-state amplitude.

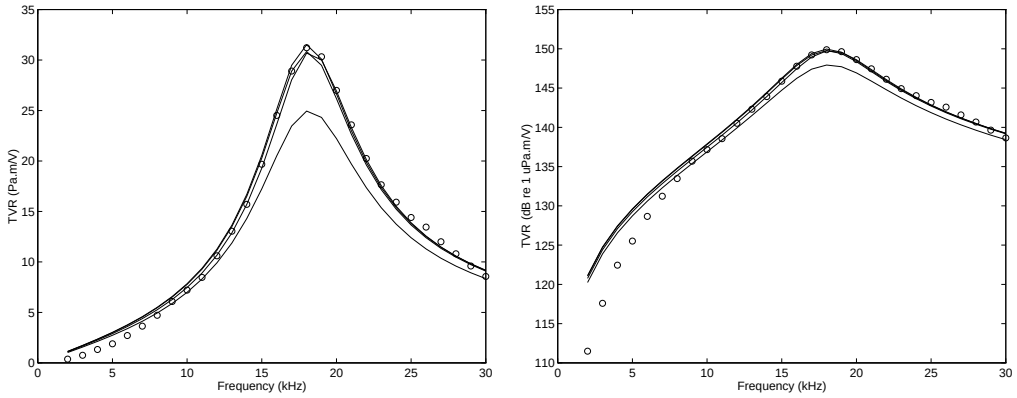

Figure 4.5 Transmitting voltage responses for an ITC1001 obtained from estimates of the resonant behaviour of the device. Each curve is derived from the analysis of data corresponding to a single drive frequency. The data analysed was contained within a time-window comprising 3 cycles of resonance frequency.

The simple model assumed above is a so-called “lumped parameter” model assuming a point projector. Modelling an extended projector using such a circuit (ie by a small number of poles and zeros) is not really valid. A more sophisticated way of modelling a transducer is to use a finite element model for the transducer. The use of *a priori* information about the transducer (for example, electrical impedance measurements, or determination of the normal modes measured in air) may be used to inform the modelling process. If measurements made in a test tank are to be used, it will be necessary to include the tank boundaries in the model. However, accurate knowledge of the acoustic properties of the tank is often difficult to obtain, thus limiting the accuracy. Nevertheless, successful attempts to use such a method to calculate the directional response of a transducer in an infinite medium from acoustic pressures measured

in an enclosed tank have been reported [4].

4.3 METHOD OF TRANSIENT SUPPRESSION

Another approach which may be used to make better use of the little echo-free signal available is to pre-condition the drive signal to the projector in such a way that no transients are excited. This would allow the steady-state to be reached immediately (or at least much more quickly) and enable measurements to be made on a part of the signal that would usually be dominated by the transient response of the projector. This method has generally been termed *transient-suppression* and has been most successfully reported in the work of Piquette [47, 48] and Giangreco [4, 11].

4.3.1 Method of Piquette

In the approach of Piquette, the main problem is in determining the correct drive voltage waveform required to stimulate the projector in such a way as to produce no transients in the sound wave radiated into the fluid medium. The goal is to produce a sound wave that is a section of a steady-state sine-wave, beginning and ending at zero-crossings of the waveform. The method of analysis involves evaluating an equivalent circuit for the projector of interest. In the case of a simple series LCR circuit, the method can be made to work exactly and complete transient suppression can be achieved. In the case of a real transducer in water, the method can only be approximate.

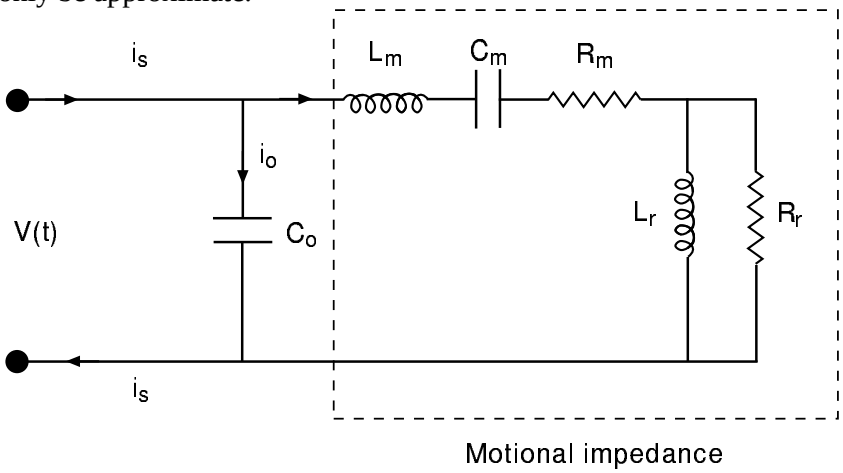

Figure 4.6 An example of an equivalent circuit for a spherical piezoelectric transducer showing circuit elements for the mechanical and radiation impedance where C_0 is the blocked capacitance, L_m, C_m and R_m are the analogues of the mechanical impedance, and R_r and L_r are the radiation load. In general, the impedance of the source must also be considered.

Figure 4.6 shows the equivalent circuit used by Piquette to model a spherical transducer in water. The circuit elements comprise a purely electrical element (the capacitor C_0), as well as elements which provide an electrical analogue of the motional part of the impedance. This circuit is more sophisticated than that in Figure 4.5 in that the motional impedance is divided into both mechanical and radiation impedance. The circuit is analysed by application of Kirchoff's laws to each circuit loop and differential equations are established describing the

circuit response. To achieve the transient suppression, Piquette chose to require the voltage across the fluid-load resistor R_r to be a perfect gated-sinusoid, this choice being based on the assumption that the pressure-wave generated by the transducer will be a scaled replica of the voltage waveform appearing across this resistor. In the case of a spherical transducer in water, the proper driving waveform consists of a sum of a pedastel voltage plus a ramp voltage plus a sinusoidal voltage which is phase-shifted with respect to the waveform that appears in the fluid.

To determine the correct values of circuit elements, the complex electrical impedance of the transducer under test is first measured as a function of frequency. A nonlinear least squares fitting algorithm is then used to determine the best-fit element values. These parameters are then used with the transient-suppression theory to generate the proper transient-suppressing drive voltage waveform. The transducer is then driven with this waveform, the waveform being generated using an arbitrary waveform generator. The pressure waveform is measured with a hydrophone and the signal digitised. A second nonlinear least squares fitting algorithm then modifies the model parameters to better fit the measured data, and the new parameters are then used to generate a new drive waveform, the process continuing iteratively until the desired degree of suppression is achieved.

This method was initially applied successfully to suppressing the transients while driving a spherical piezoelectric transducer. However, successful results have also been achieved using the same equivalent circuit with a number of other transducer types such as a flexural disc, a Helmholtz resonator, an array of piezoelectric tubes and a dual array of piezoelectric discs and squares [49]. With a modified equivalent circuit, the method has also been applied to an inductor-tuned Tonpiltz transducer and a moving-coil transducer [49], and with further refinement an electrostatic transducer [50]. A drawback of using this method is that the transient-suppressed signal emitted by the projector is generally smaller in amplitude than the unsuppressed drive signal, and the limitations of power amplifiers in faithfully reproducing the complicated drive waveforms required mean that it is difficult to drive the projectors hard enough to perform high power measurements.

4.2.2 Method of Giangreco

Giangreco has also reported applying transient-suppression methods to transducer calibration [4, 11]. In one method, a feedback system is used to constrain the velocity of the active radiating face of the transducer. The velocity is measured by monitoring the motional current in the transducer using a current transformer. A disadvantage of the method is that the values of electrical components used in the constraining feedback system must be matched to the particular transducer under test. However, this method may be used to generate very high power signals.

Another method described by Giangreco [4] involves applying a constant voltage to the transducer during the period *before* the transducer is driven with the gated sine-wave. This builds up potential energy which is transformed into kinetic energy in the ceramic when a short circuit is applied. If the steady voltage is correctly estimated and the timing of the application of the gated sine-wave is right, the discharge will supply a transient signal which

may be used to cancel out the transient generated by the start of the sinusoidal waveform. In order to get the timing of the short circuit and the value of the constant voltage correct, an analysis of the transducer equivalent circuit is performed. This method may also be used to drive the transducer with high voltage signals.

One difference between the methods of Piquette and Giangreco is that Giangreco attempts to suppress the transients in the current in the motional part of the equivalent circuit, whereas Piquette attempts to suppress the transients in the current through the radiation resistance. The implications of this distinction are not clear and require further study [4].

5. METHODS USING DIRECTIONAL RECEIVERS

Another possible approach to the calibration of transducers at low frequencies is to use a receiver which is sufficiently directional that, when aligned with the projector, it is insensitive to sound waves arriving at other angles of incidence, for example the reflections from the side walls of the measurement tank. In this way, the receiver discriminates against reflections by spatially filtering the received signal.

There are a number of potential methods to realise such a directional receiver. The fundamental requirement to achieve the required directionality is for the receiver to extend over an appropriately large area, the physical dimensions measured in acoustic wavelengths being the primary consideration. This may be accomplished in a number of ways.

5.1 LARGE AREA RECEIVER

Perhaps the simplest method conceptually is to construct a receiver with a large, continuous, planar active area. However, this is the most difficult to achieve in practice since to be useful at frequencies of only a few kilohertz, the device would need to be several metres in dimension. The practical difficulties and expense of constructing such devices mean that they are not often used in underwater acoustics. However, at the University of Bath, UK, large area hydrophones have been made from PVDF coaxial cable [51]. These have been shown to have a smooth frequency response but a complicated directional response on account of the piezoelectric anisotropy of the cable. The hydrophones have been used in combination with a parametric array for the testing the acoustic performance of materials. At the higher frequencies of 500 kHz to 10 MHz used in medical ultrasonics, large area receivers have also been constructed, for example from sheets of the piezoelectric polymer PVDF. These have been successfully used to characterise the acoustic output from ultrasonic transducers [52,53].

5.2 HYDROPHONE ARRAYS

Two examples are given of work using arrays to form directional receivers to spatially filter the sound field from a projector. Note that this description does not describe the use of near-field arrays since they are beyond the scope of this report.

5.2.1 An example of using a planar array

Another method of achieving a directional receiver is to construct a large area device from an array of small omnidirectional hydrophones. This has been attempted by a number of users, in particular by DCN, France [12,54]. The principle of the method is to create a receiving array which has a main central lobe which is directed toward the transducer under test, and nulls in the array directional response at angles where the main side wall reflections are incident. In this work, the array was generated by using two annular rings or circles of hydrophones placed coaxially about 0.3 m apart which together exhibit a dipole response. The parameters of the array (distance between rings, diameters, number of hydrophones) was studied experimentally and theoretically to reduce as much as possible the contribution from the first few reflections. The theoretical investigation of the measurement error was performed by a

source-image analysis to assess the effect of the first few echoes from the tank boundaries. The analysis concluded:

- the distance between the annuli must be approximately 0.3 m to have appropriate directivity patterns and receiving responses;
- the optimum diameter of the array depends upon the frequency - a good compromise is achieved if the diameter is equal to the acoustic wavelength;
- if the projector can be considered a point source, the predicted error is minimised for only four hydrophones in each ring.

The array described above has been used in the frequency range 500 Hz to 2 kHz in a 14 x 8 x 8 m tank to calibrate a projector which has a 12 ms transient. The array has the effect of increasing the available echo-free time of the tank by being insensitive to the initial reflections from the side walls, the array and projector being positioned to maximise this free time. However, with a dipole response, the array is still sensitive to reflections from the end walls. To reduce this, a similar array has been developed with a cardioid response, thus largely eliminating the sensitivity at an angle of 180° but at the expense of higher side lobe response.

The array was in fact a synthetic array, synthesised by moving one omnidirectional hydrophone to precise locations using a positioning carriage under computer control. The use of a synthetic array allows arrays of different sizes to be generated (which allows different frequency ranges to be measured), eliminates the need to match elements, avoids problems from diffraction around the hydrophone and cable supports, and is less cumbersome to handle. However, the measurements are more time consuming than for a fixed array.

5.2.2 An example using a synthetic line array

Recently, researchers at USRD in the USA have reported the use of techniques described as “spatial processing”. These use the variation in position of the reference hydrophone to provide some measure of discrimination between direct path signals and echoes. The method reported is analogous to the use of a line array for beam-forming [46,55].

At a given frequency of continuous-wave excitation of the projector, the acoustic pressure field is sampled by a hydrophone at a number of locations along a straight line colinear with the projector acoustic centre. This provides a set of pressures at positions along a synthetic line array. A set of weights is then calculated such that the pressure that would be seen in open water at one metre from the source is obtained from the weighted sum of the pressures at the hydrophone locations. The problem is then one of finding appropriate weights that simultaneously gives the correct pressure at one metre separation and causes the echo contributions of the weighted hydrophone responses to sum to zero. The calculation of the weights is based on simple geometrical considerations for the tank. Because of the large number of echo terms, this is in general a least-squares problem. If the tank is rectangular, an exact solution exists for the problem in terms of source-images making it easy to formulate a least squares design to calculate the weights.

In using this technique, problems have been reported with ill-conditioning in the calculations, but these can be addressed by appropriate numerical approaches. Assuming that the reflectivity of the tank walls is independent of angle can lead to an angular dependence of image contributions and if some of the hydrophone positions are far from the projector, the echo contributions may be large introducing increasing uncertainty [55].

The technique has been used in the calibration of a slotted cylinder projector with substantial improvements reported compared with the use of a single hydrophone. To improve the technique further, the array has been moved close to the projector (though this necessitates the introduction of a near-field correction) and different geometrical arrangements such as circles and cylinders have been used [55].

6. CONCLUSION

A review has been presented of different methods for calibrating underwater electroacoustic transducers in reverberant test tanks, with particular emphasis on the use of novel techniques in situations where conventional methods break down.

Techniques mentioned include the use of averaging and smoothing, using various types of noise as a source, modelling and extrapolating from the free-time signal, suppression of the transducer transient behaviour, the use of directional receivers and arrays, and attempts to model the reverberant acoustic field inside the test tank.

Results of the work on the calibration methods described has been presented in the literature, and in the case of those methods attempted at NPL, some results have been presented in this report. It is clear from these results that the accuracy of many of these methods is substantially degraded compared to what is theoretically possible from conventional methods (if a large enough volume of water were available in which to perform the calibrations). Typically, agreement with free-field calibrations varies from 0.5 to 3.0 dB depending on the method, transducer and frequency range. Although an indication has been given in this report of what are likely to be the main sources of error, a full assessment of uncertainty for each method is still required before any definitive statements may be made.

Although it is difficult to achieve the accuracy available from free-field steady-state measurements, the methods described are of great value when conducting in-house calibrations of transducers, perhaps during prototype development, where testing at sea or in open-water facilities is not practicable or too expensive.

There are a number of areas where further work would be of benefit:

- there is still clearly room for improving or fine-tuning some of the measurement techniques in question;

- an extensive assessment of the sources of error in the methods is necessary before any conclusive statements may be made about accuracy;

- a comparison could be organised by circulating examples of transducers which are particularly difficult to calibrate (for example, high-Q low-frequency projectors); each participant would calibrate the transducers using their preferred method and the results compared for each transducer;

- as a result of the above work, recommendations may be made regarding the most appropriate methods to use for particular devices in specific circumstances, with guidelines as to the procedure, sources of error and likely uncertainty.

7. AKNOWLEDGEMENTS

The work described in this report was funded by the UK Department of Trade and Industry's NMS Acoustics Programme, 1995-98. This report forms the deliverable for Project 2.1d(ii), milestone (b).

The author would like to thank Graham Dorꝺ, Geraint Green and Graham Beamiss of NPL for carrying out some of the experimental work, and Stephen Everitt of the University of Bath for the use of his impedance measurement data.

8. REFERENCES

1. IEC565: 1978. *The calibration of hydrophones*. International Electrotechnical Commission, Geneva.

2. ANSI S1.20. *Procedures for the calibration of electroacoustic transducers in water*. American National Standards Institute.

3. BOBBER, R. *Underwater electroacoustic measurements*., 1988, Peninsula Press, USA.

4. GIANGRECO, C. *Mesures acoustiques appliqu'es aux antennes sonar*, 1997, Lavoisier, France Commission, Geneva.

5. ROBINSON, S.P. and DORÉ, G.R. Uncertainties in the calibration of hydrophones at NPL by the method of three-transducer spherical-wave reciprocity, NPL Report RSA(EXT) 054, National Physical Laboratory, 1992.

6. KUTTRUFF, H. *Room Acoustics*, 1991, Elsevier (3rd edition).

7. KINSLER, L. E., FREY, A. R., COPPENS, A. B., and SANDERS, J. V., *Fundamentals of acoustics*, 1982, Wiley (3rd edition), USA.

8. EVERITT, S.J. Private communication, April, 1999. S.J. Everitt, University of Bath, UK.

9. MCMORROW, E.W., WALLACE, J.D. and COOP, J.J. Technique for rapid calibration of hydrophones using random noise fields, *Technical Memo ADC-EL41-EWM:JDW:JJC*, U.S. Navy Air Development Center, Johnsville, USA.

10. MCMAHON, G.W. and HODSON, C. Hydrophone calibration system using pseudo-random Gaussian noise signals, *Journal of the Acoustical Society of America*, **61**, 1649-1651, 1977.

11. GIANGRECO, G., FAURÉ, S. and ROSETTO, J.F. Measurement methods for low frequency transducers. *Power transducers for sonics and ultrasonics*, ed. B.F.Hamonic, O.B.Wilson and J-N. Decarpigny, Springer-Verlag, 1990.

12. GIANGRECO, G., ROSETTO, J.F. and GRANGER, C. Projector measurement techniques at low frequencies. *Transducers for Sonics and Ultrasonics*, ed. M.D. McColloum, B.F.Hamonic and O.B.Wilson, Technomic Publishing Co., 1992.

13. ROSETTO, J.F. Calibration of electroacoustic transducers working at low frequencies. DCN report no. 72824 ET/LD DU, 1992, DCN-Toulon, France.

14. KASHIWAGI, E. FM signal correlation method for underwater acoustic measurements, *Acustica*, **37**, 287-306, 1977.

15. BOGERT, B.P., HEALY, M.J.R and TUKEY, J.W. The quefrency analysis of time series for echoes: cepstrum, pseudo-autocovariance, cross-cepstrum and saphe cracking, *Proceedings of the Symposium on Time Series Analysis*, edited by M. Rosenblatt, Wiley, New York, 209-243, 1963.

16. ULRYCH, T.J. Application of homomorphic deconvolution to seismology, *Geophys*., **36**, no.4, 650-660, 1971.

17. OPPENHEIM, A.V., SHAFER, R.W. and STOCKHAM, T.G. Nonlinear filtering of multiplied and convolved signals, *IEEE Trans. Audio and Electroacoustics*, **AU-16**, no.3, September 1968.

18. RANDALL, R. B. *Application of B&K equipment to frequency analysis*, Brüel & Kjær, Denmark, 1977.

19. POCHE, L. B. Complex cepstrum processing of digitised transient calibration data for removal of echoes. NRL Report 8143, Naval Research Laboratory, USA, 1977.

20. LE GALL, Y and GAUTARD, S. Transmitting response measurement of low frequency projectors in confined environments with maximum length sequences and homomorphic signal processing. *Proceedings of the Institute of Acoustics*, **20**, pt.3, 21-28, 1998.

21. OPPENHEIM, A.V. and SHAFER, R.W. *Digital Signal Processing*, Prentice-Hall, 1974.

22. HAZELWOOD, R.A. Measuring ROV noise in test tanks. *Underwater Systems Design*, 10-16, July 1996.

23. COCHARD, N., ARZELIES, P., LACOUME, J.L and GABILLET, Y. Noise source calibration in test tank. *Proceedings of the Fourth European Conference on Underwater Acoustics*, 139-144, 1998.

24. HAZELWOOD, R.A. and ROBINSON, S.P. Acoustic power calibration in reverberant tanks. *Proceedings of the Institute of Acoustics*, **20**, pt.3, 103-110, 1998.

25. EVERITT, S.J. and HUMPHREY, V.F. Projector sensitivity measurements in reverberant fields. *Proceedings of the Institute of Acoustics*, **20**, pt.3, 111-118, 1998.

26. HEYSER, R. Acoustical measurements by time-delay spectrometry. *Journal of the Audio Engineering Society*, **15**, 370-382, 1967.

27. LUDWIG, G and BRENDEL, K. Calibration of hydrophones based on reciprocity and time-delay spectrometry. IEEE Transactions on Ultrasonics, *Ferroelectrics and Frequency Control*, **35**, 168-174, 1988.

28. GIBBS, B.M. and JONES, D.K. A simple image method for calculating the distribution of sound pressure levels within an enclosure. *Acustica*, **26**, 24-32, 1972.

29. WRIGHT, J.R. An exact model of acoustic radiation in enclosed spaces. *Journal of Audio Engineering Society*, **43**, n.10, 1995.

30. WRIGHT, J.R. Acoustic modelling of enclosed spaces. *Acoustics Bulletin*, 10-12, September 1996.

31. MCCULLOCH, C. Acoustic modelling - a personal view. *Acoustics Bulletin*, 5-11, July 1997.

32. MACEY, P.C. Comparison of transducer response in a free-field and in a tank using finite element/boundary element models. *Proceedings of the Institute of Acoustics*, **20**, pt.3, 119, 1998.

33. HARDIE, D.J.W. and ROEBUCK, I. Numerical characterisation of a reverberant tank for calibration measurements. *Proceedings of the Institute of Acoustics*, **20**, pt.3, 121, 1998.

34. PRESTON, R.C. and ROBINSON, S.P. New acoustic pressure vessel capability for the UK. *Proceedings of the Institute of Acoustics*, **20**, pt.3, 73-78, 1998.

35. BEATTY, L.G., GEORGE, J.D. and ROBINSON, J.D. Use of the complex exponential expansion as a signal representation for underwater acoustic calibration. *Journal of the Acoustical Society of America*, **63**, 1782-1794, 1978.

36. AINSLEIGH, P.L. and GEORGE, J.D. Signal modelling in reverberant environments with application to underwater electroacoustic transducer calibration. *Journal of the Acoustical Society of America*, **98**, 270-279, 1995.

37. HARRIS, P.M. and ROBINSON, S.P. Acoustic signal modelling and its application to the calibration of underwater electroacoustic transducers in reverberant environments. *Proceedings of the Institute of Acoustics*, **20**, pt.3, 13-20, 1998.

38. ROBINSON, S.P. and HARRIS, P.M. Modelling Acoustic signals in the calibration of underwater electroacoustic transducers in reverberant laboratory tanks. NPL Report CMAM 029, National Physical Laboratory, 1999.

39. MARPLE, S.L. *Digital Spectral Analysis with Applications*. Prentice Hall, Englewood Cliffs, New Jersey. 1987.

40. TRIVETT, D.H. and ROBINSON, A.Z. Modified Prony method approach to echo-reduction measurements. *Journal of the Acoustical Society of America*, 1981, **70**, 1166-1175.

41. TUFTS, D.W. and KUMARESAN, R. Estimation of frequencies of Multiple Sinusoids: Making linear prediction perform like maximum likelihood. *Proceedings of the IEEE*, 1982, **70**, 975-989.

42. OSBORNE, M.R. and SMYTH, G.K. A modified Prony algorithm for exponential fitting. *SIAM J. Sci. Comput.*, 1995, **16**, 119-138.

43. GEORGE, J.D., JAIN, V.K. and AINSLEIGH, P.L. Estimating steady-state response of a resonant transducer in a reverberant underwater environment. *IEEE International Conference on Acoustics, Speech and Signal Processing*, 1992, **5**, 1988, 2737-2740.

44. GEORGE, D.J. and GOODMAN, D.M. Application of the output error system identification method to the calibration of underwater acoustic transducers. *Underwater Acoustic Data Processing*, Kluwer Academic Publishers, 1989, 39-46.

45. GILL, P.E., MURRAY, W. and WRIGHT, M.H. *Practical Optimization*. Academic Press, 1981.

46. FORSYTHE, S.E. and AINSLEIGH, P.L. Acoustic calibration in reverberant environments: a survey of USRD measurement methodology. *Proceedings of the 16th International Congress on Acoustics and 135th meeting of the Acoustical Society of America,* 55-56, 1998.

47. PIQUETTE, J.C. Method for transducer transient suppression. I: Theory. *Journal of the Acoustical Society of America*, **92**, 1203-1213, 1992.

48. PIQUETTE, J.C. Method for transducer transient suppression. II: Experiment. *Journal of the Acoustical Society of America*, **92**, 1214-1221, 1992.

49. PIQUETTE, J.C. Applications of the method of transducer transient suppression to various transducer types. *Journal of the Acoustical Society of America*, **94**, 646-651, 1993.

50. PIQUETTE, J.C. A fully mechanical linear transducer model with application to generalising the nonlinear Hunt electrostatic transducer for harmonic and transient suppression. *Journal of the Acoustical Society of America*, **98**, 422-430, 1998.

51. HUMPHREY, V.F., SIMMONDS, D.J. and GREEN, M. Large area PVDF coaxial cable hydrophones. *Proceedings of the Second European Conference on Underwater Acoustics*, 567-572, 1994.

52. COSTA, E.T., LEEMAN, S. and HODDINOTT, J.C. Results of a new approach towards measurement of ultrasound characteristics. *Proceedings of Ultrasonics International 87*, 502-508, 1987.

53. ZEQIRI, B. Field parameter measurements using a large-aperture hydrophone. *Proceedings of Ultrasonics International 89*, 989-994, 1989.

54. GIANGRECO, C., ROSSETTO, J.F. and RIPOLL, Y. Measurement methods for low frequency transducers. *Proceedings of Undersea Defence Technology*, 88-90, 1991.

55. FORSYTHE, S.E., AINSLEIGH, P.L. and PIQUETTE J.C. A synthetic array technique for calibrating resonant transducers. *Proceedings of the Institute of Acoustics*, **20**, pt.3, 39-46, 1998.

APPENDIX A : MODAL DENSITY IN A REVERBERANT TANK

The wave equation for an enclosed space yields non-zero solutions only for certain discrete values of the wave number. These values are termed eigenvalues, and each corresponding solution is known as an eigenfunction, or *normal mode* of the enclosure. The corresponding frequencies are called eigenfrequencies or *resonance frequencies*. For a rectangular enclosure, the number of eigenfrequencies, N_f, from 0 up to a frequency f is given by [6].

$$N_f = \frac{4\pi}{3} V \frac{f^3}{c^3}$$

where V is the volume of the enclosure and c is the speed of sound. The average density of eigenfrequencies on the frequency axis (ie the number of eigenfrequencies per Hz) at the frequency f is

$$\frac{dN_f}{df} = 4\pi\ V \frac{f^2}{c^3}$$

where the symbols are the same as for the equation above. Therefore, for the small NPL tank of dimensions 1.5 x 1.5 x 2.0 m, there are roughly 6700 modes in a 1 kHz band centred on 20 kHz. It should be noted that the expression in the equation for N_f is an approximation which slightly underestimates the number of modes [6]. It can also be shown [6] that a lower limit of frequencies, f_g, where a statistical treatment of superimposed normal modes in a room is permissible is given by:

$$f_g = 2000 \sqrt{\frac{T}{V}}$$

where T is the reverberation time.

APPENDIX B: ACOUSTIC PRESSURE IN REVERBERANT FIELDS

B1 DIRECT SOUND PRESSURE

It can be shown [7] that the square of the sound pressure arriving direct from a spherically-spreading source is given by:

$$P_d^2 = \frac{\rho_0 c}{4\pi r^2} W$$

where P_d is the effective (or RMS) direct sound pressure, r is the distance from the source (measured to the acoustic centre), ρ_0 is the density of the medium, c the speed of sound in the medium, and W is the total acoustic power output of the source.

Note that the expression is derived assuming that the sound field is radiated uniformly in all directions.

B2 REVERBERANT SOUND PRESSURE

By consideration of the energy density in the reverberant sound field, it is possible to derive the following expression[6, 7] for the reverberant sound pressure, P_r :

$$P_r^2 = \frac{4\rho_0 c}{A} W$$

where ρ_0 and c are defined as above, W is once again the total acoustic power of the source, and A is defined as the *total sound absorption* of the room (or tank). The latter quantity has the units of m^2 (sometimes referred to as *metric sabin*). Note also that P_r is defined as the spatially averaged effective pressure amplitude of the reverberant sound field and is defined as $(\Sigma P_i^2)^{½}$ ie the square root of the sum of the squares of the RMS pressures of all the individual rays which arrive at a given point.

There are a number of assumptions which have been made to derive the expression above. The theory is derived from considering the steady-state energy density, so the expression above applies only after the reverberant field has built up to its steady-state value. There is assumed to be an ideally diffuse distribution of acoustic energy. For this purpose, we assume that the incident waves are distributed uniformly over all possible directions of incidence, so that each element of solid angle carries the same intensity. Furthermore, we can assume that the phases of the elementary waves are distributed at random so that interference effects can be neglected and we can simply add their energies (proportional to the square of the pressure amplitudes).

This is only valid for a room or tank which is highly reverberant (the walls are highly reflective). If substantial absorption is present in the walls, the first reflection will be significantly larger in amplitude and will dominate over the subsequent arrivals. In this case, the application of the statistical theory of reverberations becomes highly questionable. It may also break down at low frequencies where the number of modes per hertz is reduced, so that certain modes predominate[7].

B3 TOTAL SOUND PRESSURE

The total mean squared pressure, P_t, originating from the direct and reverberant field can be found by adding the expressions in equation (1) and (2) to obtain:

$$P_t^2 = \rho_0 cW\left(\frac{1}{4\pi r^2} + \frac{4}{A}\right)$$

Note that close to the source, where $4\pi r^2 << (A/4)$, the direct field is dominant. However, for distances where $4\pi r^2 >> (A/4)$, the effect of the reverberant field is the major contribution. Note that (once steady-state has been reached) the reverberant field is a constant background level determined by ρ_0, c, W and A, but *independent* of r.

APPENDIX C: TYPES OF ACOUSTIC MODELLING

Crudely speaking, it is possible to divide modelling techniques into three broad classes:

- (semi) empirical methods,
- numerical methods (based on equations for the physics of vibro-acoustics), such as finite elements and boundary elements
- geometrical or energy-distribution-based methods, such as ray tracing,

C1 EMPIRICAL METHODS

A number of rules and formulæ are in use in the treatment of room reverberation in classical acoustics, for example Sabine's and Eyring's room reverberation formulæ. These rules and formulæ are generally well-tested, in the sense that they have been developed over many years and have usually been refined and adjusted when measurements and practical experience demanded it. The formulæ are almost always devised so as to be practical for "hand" calculation. Typically, they are published in literature, national or international standards. These formulæ can be programmed into computer codes, in some cases as simple as a spreadsheet.

C2 GEOMETRICAL OR ENERGY METHODS

Modelling methods of these types rely on some geometrical description of the sound field together with formulæ which describe the physics of propagation. There is usually a distinction made between purely acoustic methods (eg ray tracing) and vibro-acoustic methods (such as statistical energy analysis). The latter can include acoustic regions, but is usually mainly concerned with structural vibration.

In the method of ray tracing, the propagation of the sound is calculated assuming that it can be considered as a ray or beam of acoustic energy, undergoing reflection at any surface it meets. Normally, the reflection is considered specular (the surface being regarded as a plane mirror) but diffuse reflections may also be included. Essentially, the trace of the ray (or beam centre-line) locates mirror images of the sources, to some user-controlled order of reflections, taking into account the visibility of each surface from the previous image source. There is usually a trade off between accuracy and number of images taken into account. Absorption takes place at surfaces, and in the medium along the path if required. Sound energy arriving at some receiver location is added in a standard energy sense to arrive at steady-rate behaviour, or the impulse response can be derived from the path lengths (and hence travel time) of the rays to arrive at reverberation time, etc.

Ray/beam tracing has a number of limitations, a main one being due to the assumption that the sound can be considered as energy being distributed as a result of reflections. In other

words, wave phenomena such as diffraction, refraction and interference are not taken into account. This limits the applicability to the higher frequency ranges (more precisely, above the Schroeder cut-off frequency, or where there are many, overlapping, room modes). Recently, more advanced features have even removed this limitation through the use of phase ray tracing. Wave effects may be accounted for by simple or complex formulæ for diffraction, or by considering phase content (based on ray path length) as well as energy level in each ray, and adding-up energy in a complex (amplitude and phase) sense. Advanced models may include absorption, reflection and diffusion at surfaces.

C3 NUMERICAL METHODS

Numerical methods includes any modelling approach in which the physics of vibro-acoustics or sound propagation is modelled by equations describing the fundamental phenomena, essentially wave propagation. The equations are solved in numerical form, typically by some sort of discretisation of the geometry into elements and the assembly of a matrix equation system using numerical integration. The two most common approaches are the finite element and the boundary element methods.

The finite element (FE) method divides the acoustic medium into volume elements (for a 3-d problem) which are typically bricks, prisms or tetrahedra. The boundary element (BE) method divides the medium in a two-step approach: the wave behaviour in the (3-d) fluid is first condensed to a (2-d) surface integral problem and the surface is divided into elements, which are typically quadrilaterals or triangles. The BE method can therefore directly handle exterior, open, field problems, whereas FE can only do so by introducing approximations at some finite boundary.

The typical approach adopted in numerical acoustics is to model the propagation of acoustic waves by an equation, typically the Helmholtz form of the wave equation which involves functions of frequency rather than time. By dividing-up the medium (water etc) into elements, the equation in the continuum is broken-down into a matrix equation, which can be solved numerically rather than analytically. Finite elements divide the medium directly into elements. Boundary elements divide the boundary surfaces into elements and use further mathematics (based on, for example, Green's theorem) to condense the 3-d field problem to a 2-d surface integral problem.

Since FE is by definition finite, it is limited to closed regions. BE can handle interior, closed, regions, or exterior, open, regions - or, using the indirect, variational form of the BE equations, it can also handle mixed regions, where the interior is linked to the exterior through relatively small openings, or through the walls of a flexible structure.

The effect of a flexible structure can be taken into account by coupling the FE or BE acoustic model to a structural FE model (which may use a different mesh of elements, depending on the nature of the structural details which ought to be taken into account). An efficient procedure for fluid-structure coupling uses the (uncoupled) modes of the structure to define the structural behaviour, rather than the complete mass and stiffness matrices, since this leads to a much smaller size of the coupled equation system. Structural damping can be included,

as well as acoustic absorbers.

The excitation of the acoustic or vibro-acoustic system can be defined as vibrations of a boundary structure, or applied forces on a flexible structure, or acoustic wave sources. Normally, all excitations are coherent, since we are solving a deterministic set of equations.

The results consist of acoustic pressures and velocities on the boundary surfaces and at all points in the field. These data are complex and frequency-dependent. (All calculations are carried out at discrete, narrow-band, frequencies). Since the results are complex values with amplitude and phase, acoustic intensities can also be computed, together with radiated sound power, through a defined surface or from the object as a whole. Diagrams of directivity, and frequency plots showing the contributions to be radiated energy from different parts of the object can also be produced.

FE and BE can be used for any acoustic models where wave phenomena predominate. The field is being divided into elements, or in other words the waves are “sampled” in space, hence there must be sufficient sampling points (notes of the element mesh) to avoid “spatial aliasing”. This normally implies a minimum of about 6 linear elements per wavelength. Thus for any particular fineness of mesh, there is a nominal maximum frequency for which the results have acceptable accuracy. (This simple rule ignores any further refinement which may be needed due to small gaps between parts, getting a correct representation of a structural vibration shape, and other aspects). The maximum frequency is, of course, a limit at which accuracy starts to deteriorate significantly, not a fixed limit. Consequently, to model any particular frequency range, the mesh density can be established, and hence the numbers of nodes and elements for an object of a given size. As mesh density increases, so does storage space and computer time so there is a practical limit to the frequencies which can be considered. In addition, the assumptions of coherent, interacting waves, may begin to break down as the acoustic modal density or modal overlap increases, giving another upper frequency limit, based on what is the correct approach to model the physics of the behaviour. At this limit, the use of ray/beam tracing should be considered. The surface properties (phase shifts in absorbers, vibration phase etc) may also not be properly known in a deterministic way at higher frequencies